

Insights into the physical properties of a new 211 MAX phase Nb₂CuC

Hadi, M. A., Kelaidis, N., Naqib, S. H., Islam, A. K. M. A., Chroneos, A. & Vovk, R.

Author post-print (accepted) deposited by Coventry University's Repository

Original citation & hyperlink:

Hadi, MA, Kelaidis, N, Naqib, SH, Islam, AKMA, Chroneos, A & Vovk, RV 2021, 'Insights into the physical properties of a new 211 MAX phase Nb₂CuC', Journal of Physics and Chemistry of Solids, vol. 149, 109759.

<https://dx.doi.org/10.1016/j.jpcs.2020.109759>

DOI 10.1016/j.jpcs.2020.109759

ISSN 0022-3697

Publisher: Elsevier

NOTICE: this is the author's version of a work that was accepted for publication in Physics and Chemistry of Solids. Changes resulting from the publishing process, such as peer review, editing, corrections, structural formatting, and other quality control mechanisms may not be reflected in this document. Changes may have been made to this work since it was submitted for publication. A definitive version was subsequently published in Journal of Physics and Chemistry of Solids, 149, (2021) DOI: 10.1016/j.jpcs.2020.109759

© 2021, Elsevier. Licensed under the Creative Commons Attribution-NonCommercial-NoDerivatives 4.0 International <http://creativecommons.org/licenses/by-nc-nd/4.0/>

Copyright © and Moral Rights are retained by the author(s) and/ or other copyright owners. A copy can be downloaded for personal non-commercial research or study, without prior permission or charge. This item cannot be reproduced or quoted extensively from without first obtaining permission in writing from the copyright holder(s). The content must not be changed in any way or sold commercially in any format or medium without the formal permission of the copyright holders.

This document is the author's post-print version, incorporating any revisions agreed during the peer-review process. Some differences between the published version and this version may remain and you are advised to consult the published version if you wish to cite from it.

Insights into the physical properties of a new 211 MAX phase Nb₂CuC

M.A. Hadi^{1*}, N. Kelaidis², S.H. Naqib¹, A.K.M.A. Islam^{1,3}, A. Chroneos,^{2,4} R.V. Vovk⁵

¹Department of Physics, University of Rajshahi, Rajshahi 6205, Bangladesh

²Faculty of Engineering, Environment and Computing, Coventry University, Priory Street, Coventry CV1 5FB, UK

³International Islamic University Chittagong, Kumira, Chittagong 4318, Bangladesh

⁴Department of Materials, Imperial College, London SW7 2AZ, UK

⁵V. Karazin Kharkiv National University, 4 Svobody Square, Kharkiv, 61077, Ukraine

ABSTRACT

A systematic density functional theory study with two functionals –generalized gradient approximation (GGA) and local density approximation (LDA)–is carried out to explore the structural, electronic, elastic, thermal, vibrational and optical properties of a new 211 MAX phase Nb₂CuC. To facilitate comparison we also study Nb₂AlC, the precursor of Nb₂CuC. The calculated band structures reveal the metallic conductivity of both compounds. The replacement of Al with Cu modifies the band profiles of Nb₂CuC and consequently leads to its improved physical properties. Considering the position of the Fermi level on the total density of states (DOS), the new compound Nb₂CuC is structurally less stable than Nb₂AlC. The total DOS at the Fermi level obtained with GGA is slightly larger than those obtained with LDA. The Nb–C and Nb–A (A = Cu/Al) are covalent bonds, and Nb–Nb bonds lead to antibonding states in both MAX phases. The charge transfer among constituent atoms indicates some ionic character in the chemical bonds of Nb₂CuC and Nb₂AlC. Both MAX phases are mechanically and dynamically stable. The Nb₂CuC is ductile and consequently damage tolerant, whereas Nb₂AlC is brittle. However, Nb₂CuC is relatively soft and machinable. In most cases Nb₂CuC is more elastically anisotropic than Nb₂AlC, and Nb₂CuC is expected to be a promising thermal barrier coating material. We propose that Nb₂CuC is a better coating material for preventing solar heating than Nb₂AlC, and Nb₂CuC is expected to be superconductive because its Fermi surface has a nesting nature.

Keywords: New MAX phase; Mechanical properties; Electronic structure; Optical functions

1. Introduction

The MAX phases (M_{n+1}AX_n, where M is early transition metals, A is A-group elements and X is C or N or B, n=1,2,3...) are ternary carbides, nitrides and borides and form a family of more than 80 members [1–4]. The MAX phases crystallize in the hexagonal space group *P6₃/mmc* (194). The unit cell contains M₆X-octahedra with the X-elements filling the octahedral positions between the M-elements, which are the same as those originating in the corresponding MX binaries. The octahedra alternate with the A-atomic layers positioned at the centers of trigonal prisms, which are somewhat larger, and therefore more accommodating of the larger A-atoms. The intercalating pure A-atomic planes are mirror planes to the zigzagging ceramic M_{n+1}X_n slabs. These alternating metallic and ceramic layers in MAX phases give them a unique set of metallic and ceramic properties [5]. The typical metallic properties are high electrical and thermal conductivities, high fracture toughness, machinability, damage tolerance and resistance to thermal shock. The ceramic-like properties are lightweight, resistance to oxidation and corrosion, elastic rigidity, fatigue tolerance and maintaining strength at high temperatures [6]. The MAX phases can undergo plastic-to-brittle transitions at elevated temperatures, and the compounds can withstand high compressive stresses at ambient temperature [7]. Due to these remarkable properties they have potential uses as coatings for electrical contacts, thermal shock refractories and heating elements at high temperature [8]. In addition, they have potential nuclear applications as they are neutron irradiation resistant and can be used as precursors for production of two-dimensional MXenes [9].

Some new numbers of MAX phases were recently synthesized through replacement reaction between MAX phase precursors and molten salts [10]. Furthermore, Ding *et al.* [11] synthesized the new phase Nb₂CuC by A-site replacement reaction in a molten salt environment. In the new compound, the A-group element Al in Nb₂AlC is replaced with the transition metal Cu. Transition metals (having d-orbital electrons) possess unique properties that differ from A-group elements. The introduction of late-transition metals into the A layer has the potential to tailor the physical properties of the MAX phases. In this study, the structural, elastic, electronic, dynamic, thermal and optical

* Corresponding author: hadipab@gmail.com

properties along with theoretical Vickers' hardness of the newly synthesized Nb₂CuC MAX phase are investigated.

2. Methodology

The CASTEP code [12] based on density functional theory (DFT) [13,14] is used for all calculations. For the local density approximation (LDA) calculations, the CA-PZ functional [15,16] is used; whereas for the generalized gradient approximation (GGA), the PBE functional is chosen [17,18]. Vanderbilt-type ultrasoft pseudopotential is applied to model the interaction of electrons with ion cores [19]. The valence electronic configurations are presented by 2s²2p² states for C, 3d¹⁰4s¹ states for Cu, 3s² 3p¹ states for Al and 4s²4p⁶4d⁴5s¹ states for Nb. To minimize the total energy and internal forces, the Broyden–Fletcher–Goldfarb–Shanno scheme [20] is employed. Convergence calculations showed that a 550 eV plane-wave cutoff energy is appropriate. For the sampling of the Brillouin zone integration, a k-point mesh of 10×10×2 grid is used according to the Monkhorst–Pack scheme [21]. Geometry optimization is accomplished with the following convergence criteria: 5×10⁻⁶ eV for total energy, 0.01 eV/Å for maximum force, 0.02 GPa for maximum stress and 5×10⁻⁴ Å for maximum displacement. The charge density and Fermi surface (FS) require denser k-points and thus a 37×37×8 grid k-point is used for these calculations.

The elastic constants C_{ij} are calculated using finite-strain theory [22] as implemented in the CASTEP code. This method is widely used for all kind of crystals [23–35]. According to this theory, a given set of identical deformations (strains) is applied to the conventional unit cell, accepting the relaxation of the atomic degrees of freedom. After that the resulting external stresses are estimated. The stress tensor has six stress components σ_{ij} for each strain δ_j applied to the unit cell. The elastic constants C_{ij} are then determined by solving a set of linear equations, $\sigma_{ij} = C_{ij}\delta_j$.

The Mulliken population analysis [36] within this code is performed using Mulliken formalism modified with the projection of plane-wave states onto a localized basis via the technique by Sanchez-Portal *et al.* [37]. Lattice dynamical properties are determined using the finite displacement supercell method based on perturbation DFT. The dimension of supercell is fixed with the cutoff radius of 3.0 Å, resulting in a supercell (32 atoms) of volume four times that of the unit cell.

The imaginary part of the dielectric constant leads to the calculation of other optical functions of crystalline solids. The following expression is used to calculate the imaginary part of the dielectric function:

$$\varepsilon_2(\omega) = \frac{2\pi e^2}{\Omega \varepsilon_0} \sum_{k,v,c} |\psi_k^c| \mathbf{u} \cdot \mathbf{r} |\psi_k^v|^2 \delta(E_k^c - E_k^v - E) \quad (1)$$

where ω is the phonon frequency, e is the charge of an electron, Ω is the unit cell volume, \mathbf{u} is the unit vector along the polarization of the incident electric field and ψ_k^c and ψ_k^v are wavefunctions for conduction and valence band electrons at a particular k-vector, respectively. The expressions for other functions are available in literature [38].

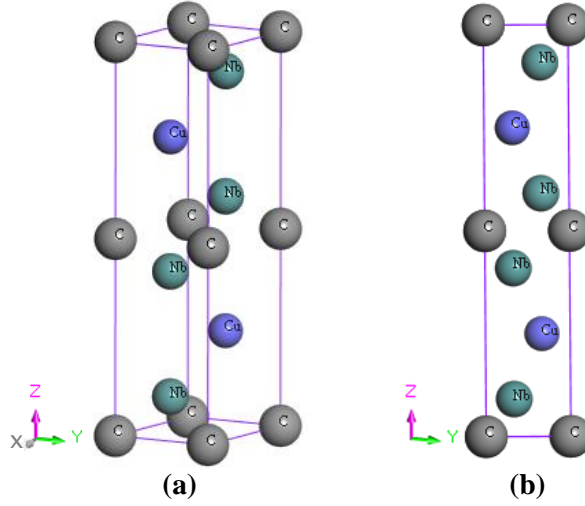
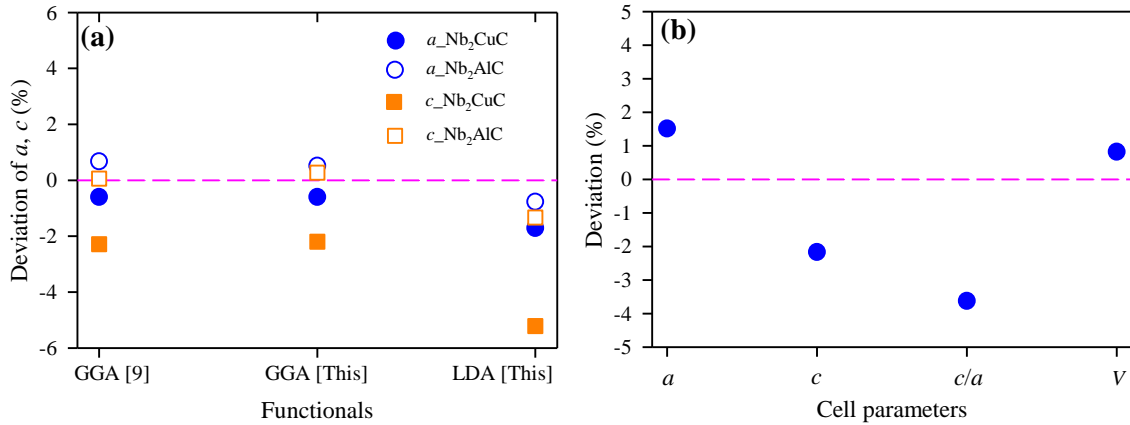
3. Results and discussion

3.1. Structural properties

The geometric structure of Nb₂CuC is shown in Fig. 1. The calculated structural properties of Nb₂CuC and Nb₂AlC are listed in Table 1 along with the experimental and other theoretical values to facilitate comparison. The present values, particularly the GGA values are consistent with the experimental and previous GGA results (Fig. 2a). The LDA is known to underestimate the lattice parameters and consequently the cell volume. The replacement of A-group element Al from Nb₂AlC by Cu reduces the lattice constant c in both experiment and theoretical studies. The lattice constant a of Nb₂CuC is slightly larger than that of Nb₂AlC in the experiment and GGA studies. The LDA result for a of Nb₂CuC is rather small compared with the experiment and slightly larger than the LDA value of Nb₂AlC. The A-site replacement reaction through molten salt modifies both the lattice parameters a and c of Nb₂CuC, affecting the cell volume by a small amount (Fig. 2b).

Table 1. Structural properties of Nb₂CuC and Nb₂AlC.

Compound	<i>a</i>	<i>c</i>	<i>c/a</i>	<i>V</i>	Remarks
Nb ₂ CuC	3.153	13.587	4.309	116.98	Experiment [11]
	3.134	13.276	4.236	112.93	GGA [11]
	3.134	13.288	4.230	113.01	GGA [present study]
	3.099	12.878	4.156	107.13	LDA [present study]
Nb ₂ AlC	3.106	13.888	4.471	116.03	Experiment[39]
	3.127	13.896	4.444	117.67	GGA [11]
	3.122	13.926	4.461	117.56	GGA [present study]
	3.082	13.703	4.446	112.72	LDA [present study]

**Fig. 1.** The geometric structure of Nb₂CuC: (a) 3D view and (b) 2D view.**Fig. 2.** (a) Deviation of calculated lattice parameters from experimental values and (b) deviation of experimental cell parameters of Nb₂CuC compared with Nb₂AlC.

The deviation of calculated lattice parameters from their experimental values (Fig. 2a) indicates that both *a* and *c* deviate more for Nb₂CuC than for Nb₂AlC. However, according to the trend, LDA values deviate more than those derived using GGA. Fig. 2b shows the substitutional effects of Al by Cu on cell parameters of Nb₂CuC. The lattice parameter *a* and cell volume *V* increase by 1.51% and 0.82%, respectively, whereas the lattice constant *c* decreases by 2.17% when Al is replaced by Cu from Nb₂AlC. This means that, in the new compound Nb₂CuC, bond strength along the *c*-axis increases and along the *a*-axis decreases compared with Nb₂AlC. Generally, the lattice parameters will increase when a smaller atom is replaced with a larger one. However, the ionic radius, valence state and electron affinity are also important factors that decide bond length and consequently lattice parameters. If a system has high electron affinity, it reduces the bond length and hence decreases lattice parameters. In the present case, Cu (1.236 eV) has huge electron affinity compared with Al (0.4328 eV). Along the *c*-axis, one Cu atom pulls two Nb atoms residing at its both sides. Consequently, the lattice parameter *c* decreases.

3.2. Electronic properties

3.2.1. Band structure and density of states

The electronic band structures for Nb_2CuC and Nb_2AlC are calculated with LDA and GGA functionals and are shown in Figs. 3 and 4, respectively. The band profiles of Nb_2CuC calculated with LDA and GGA functionals are similar. Many valence bands accumulate at the Γ -point around the Fermi level (E_F) for both compounds, calculated using two different functionals. In both profiles, the valence and conduction bands overlap considerably and as a result no band gap appears. Therefore, Nb_2CuC is a metallic compound similar to the typical MAX phases [1,6,38,40–48]. The LDA and GGA band profiles of Nb_2AlC are very similar to those of Nb_2CuC ; nevertheless, there are clear differences between these two sets of band profiles. The substitution of Al with Cu modifies the band profiles of Nb_2CuC . Lower as well as higher valence bands in Nb_2CuC shift toward E_F . A large number of valence bands accumulate around -3 eV regions. Along the Γ -point, both valence and conduction bands condense toward E_F . The modified band structure should lead to improved physical properties of Nb_2CuC . The purely valence and conduction bands are identified with purple and light blue, respectively. The crossing and overlapping bands are indicated with orange color.

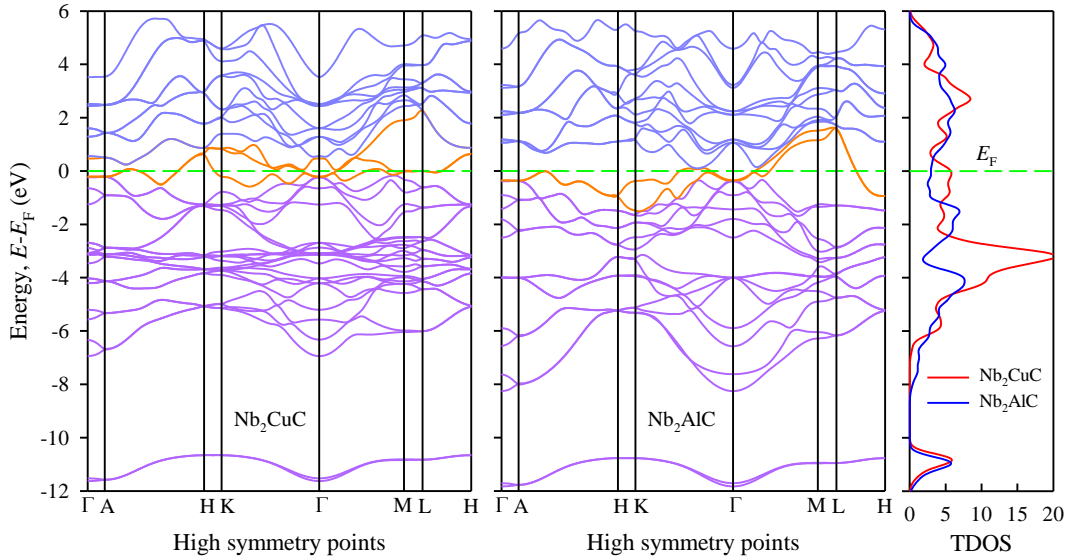


Fig. 3. Electronic band structure of Nb_2CuC and Nb_2AlC calculated with LDA functional.

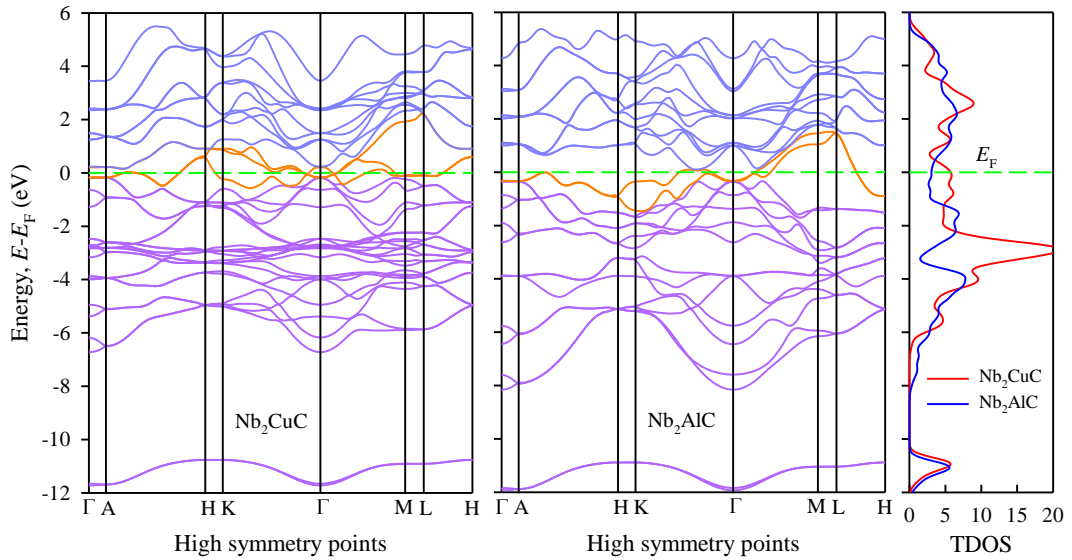


Fig. 4. Electronic band structure of Nb_2CuC and Nb_2AlC calculated with GGA functional.

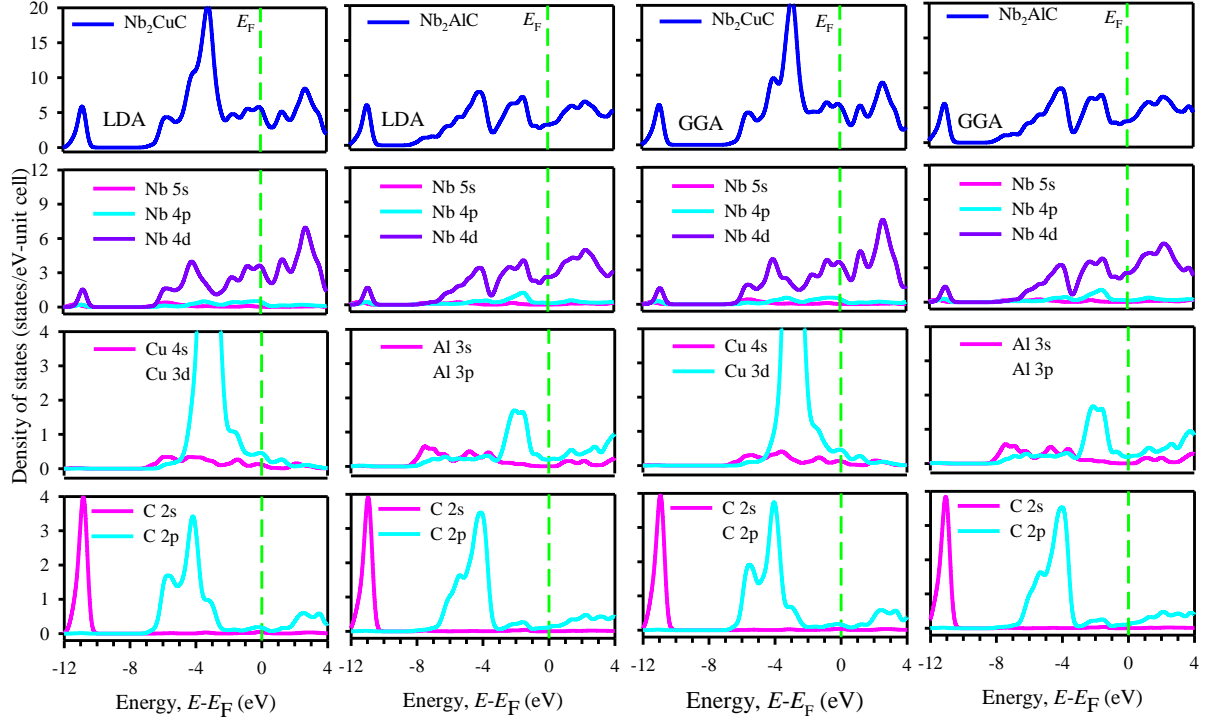


Fig. 5. Electronic DOS of Nb₂CuC and Nb₂AlC calculated with LDA and GGA functionals.

The density of states (DOS) of Nb₂CuC and Nb₂AlC are calculated using LDA and GGA functionals (Fig. 5). As found for the band structures, both LDA and GGA DOS profiles of Nb₂CuC and Nb₂AlC are similar. However, the DOS profiles of Nb₂CuC distinctly differ from those of Nb₂AlC. The E_F of Nb₂CuC is situated at a peak, whereas the E_F of Nb₂AlC is at a dip on the left side of a pseudogap of the total DOS, indicating that Nb₂CuC is structurally less stable than Nb₂AlC [49,50]. Consequently, Nb₂CuC has higher total DOS at E_F compared with Nb₂AlC. The total DOS $N(E_F)$ at E_F , obtained with LDA and GGA for Nb₂CuC are 5.69 and 5.73 states/eV-unit cell, respectively, and correspondingly for Nb₂AlC are 2.92 and 3.05 states/eV-unit cell. The GGA values are slightly larger than those obtained from LDA calculations. There are no values in the literature for Nb₂CuC. The previously reported LDA values of $N(E_F)$ for Nb₂AlC are 3.84 and 3.78 states/eV-unit cell [51,52], and the GGA values are 3.40 and 3.36 states/eV-unit cell [53,54]. Both LDA and GGA values found in the literature are comparable with the present values. Although the functionals are the same, the parameterizations and computational codes differ between the present and previous studies [34–37]. The literature LDA values are slightly larger than GGA values, which is opposite of the present study. The general trend of LDA or GGA for total DOS at E_F is still unknown, and we aim to analyze this issue in a following paper. The experimental total DOS of Nb₂AlC is 5.06 states/eV-unit cell [52], which is very large compared with the present and previous results. The experimental results depend on the purity of the sample. Barsoum *et al.* [55] measured total DOS at E_F for Nb₂SnC as 2.66 states/eV-unit cell, whereas Lofland *et al.* [52] found 4.84 states/eV/unit-cell.

Lower valence bands in Nb₂CuC and Nb₂AlC consist of C 2s and Nb 4d orbitals, indicating strong covalent Nb–C bonds according to both LDA and GGA calculations. The higher valence band of Nb₂CuC consists of a high peak with two arms at the left and an uneven part spreading up to E_F . The first and second arms arise due to hybridization between C 2p and Nb 4d states. The peak mainly originates from the Cu 3d states along with a few contributions of Nb 4d states. The arms and peak lead to Nb–C and Nb–Cu covalent bonds, respectively. Conversely, the higher valence band of Nb₂AlC is divided into the two distinct low peaks: the first due to hybridization between C 2p and Nb 4d electrons; and the second adjacent to E_F originates from the interaction of Al 3p and Nb 4d orbitals. These two peaks correspond to the Nb–C and Nb–Al covalent bonds, respectively. The Nb 4d states mainly contribute to the total DOS at E_F . The d-resonance at E_F is the origin of metallic conductivity of Nb₂CuC and Nb₂AlC. The Nb₂CuC is expected to be more metallic than Nb₂AlC as d-resonance at E_F is stronger in Nb₂CuC than in Nb₂AlC.

Because the new compound Nb₂CuC has an additional transition metal Cu at the A-site, the spin polarization calculations are performed for electronic band structure and DOS. These calculations show no effect of considering spin polarization on electronic band structure and DOS (data not shown). Electronic structure controls most of the physical properties of a compound. Therefore, we conclude that the elastic, thermal and optical properties of Nb₂CuC will not be affected if spin polarization is considered.

3.2.2. Mulliken atomic and bond populations

The calculated Mulliken atomic populations are listed in Table 2. Mulliken charge leads to quantifying the effective valence, which is the absolute difference between the formal ionic charge and the Mulliken charge on the atomic species. A zero value of effective valence is associated with a perfect ionic bond, and a value greater than zero indicates an increasing level of covalency. The results with both functionals are similar and show that the chemical bonding in Nb₂AlC has a higher covalent character compared with Nb₂CuC. The Mulliken charge assigned to A-group element Cu is negative, whereas Al has positive charge. In both compounds, C has negative charge and Nb has positive charge. In Nb₂CuC, Nb transfers its electronic charge and Cu and C receive this charge; whereas in Nb₂AlC, Nb and Al transfer their electronic charges and C accepts these charges. The charge transfer indicates the ionic character in the chemical bond of Nb₂CuC and Nb₂AlC.

Table 2. Mulliken atomic populations, Mulliken charge, ionic charge and effective valence

Phases	Functional	Atoms	Mulliken atomic populations				Mulliken charge ($ e $)	Ionic charge ($ e $)	Effective valence ($ e $)
			s	p	d	Total			
Nb ₂ CuC	LDA	C	1.45	3.25	0.00	4.70	-0.70	+4.00	3.30
		Cu	0.76	0.91	9.66	11.34	-0.34	+2.00	1.64
		Nb	2.24	6.36	3.89	12.48	0.52	+5.00	4.48
	GGA	C	1.46	3.24	0.00	4.70	-0.70	+4.00	3.30
		Cu	0.70	0.91	9.67	11.27	-0.27	+2.00	1.77
		Nb	2.23	6.45	3.83	12.51	0.49	+5.00	4.51
Nb ₂ AlC	LDA	C	1.45	3.24	0.00	4.69	-0.69	+4.00	3.31
		Al	0.97	1.84	0.00	2.81	0.19	+3.00	2.81
		Nb	2.21	6.53	4.01	12.75	0.25	+5.00	4.75
	GGA	C	1.46	3.23	0.00	4.69	-0.69	+4.00	3.31
		Al	0.97	1.83	0.00	2.80	0.20	+3.00	2.80
		Nb	2.22	6.58	3.95	12.75	0.25	+5.00	4.75

Table 3. Mulliken bond populations P^{μ} with bond number n^{μ} and bond length d^{μ} .

Bond	Functional	Nb ₂ CuC			Nb ₂ AlC		
		n^{μ}	$d^{\mu}/\text{\AA}$	P^{μ}	n^{μ}	$d^{\mu}/\text{\AA}$	P^{μ}
Nb-C	LDA	4	2.15293	0.98	4	2.15657	0.97
	GGA	4	2.17651	1.01	4	2.18220	1.00
Nb-A	LDA	4	2.70030	0.44	4	2.83526	0.52
	GGA	4	2.78112	0.42	4	2.88429	0.55
Nb-Nb	LDA	2	2.98905	-0.43	2	3.01738	-0.57
	GGA	2	3.02125	-0.41	2	3.04962	-0.57

Mulliken bond overlap population is an additional tool to predict the bonding nature of crystalline solids. The electron clouds between two atoms lead to a bond overlap population. A bond population closer to the zero value indicates the increasing level of ionicity and a perfectly ionic bond has an exact zero value. A positive bond population is always associated with a covalent bond and covalency increases with the increase of bond population. Negative bond populations refer to the antibonding states between the relevant pairs of atoms. Mulliken bond populations calculated for Nb₂CuC and Nb₂AlC are listed in Table 3, indicating that Nb-C and Nb-A (A = Cu/Al) are covalent bonds and Nb-Nb bonding leads to antibonding states in both MAX phases. The Nb-C bond in Nb₂CuC is more covalent than that in Nb₂AlC due to the larger bond population. Conversely, Nb-Al bonding in Nb₂AlC is more covalent than the similar Nb-Cu bond in Nb₂CuC in the view of bond population.

3.2.3. Charge density map and FS

A charge density (CD) map visualizes the charge density distribution of an atom within a crystal, which is the difference per unit volume between its nuclear positive charge and its electronic negative charge. The CDs of the atoms are responsible for their electrostatic potential (ESP) distributions. A CD map is easier to interpret than an ESP map because it is less sensitive to long-range electrostatic effects. The CD maps of Nb₂CuC and Nb₂AlC calculated for the (110) plane using GGA and LDA are shown in Fig. 6.

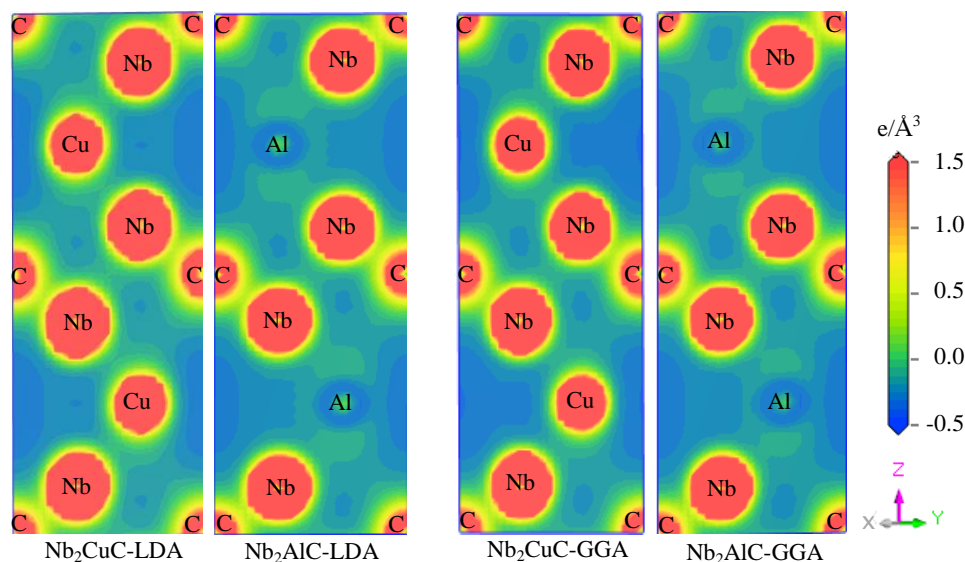


Fig. 6. Electron charge density maps of Nb₂CuC and Nb₂AlC in (110) plane.

The CD map clearly shows that the charge around Cu (11.34/11.27e) is higher than that around Al (2.81/2.80e) according to GGA/LDA calculations. The overlapping of the electron cloud between the Nb and C atoms indicates the strong covalent Nb–C bond in Nb₂CuC and its precursor Nb₂AlC. The charge overlap between Nb and Al in Nb₂AlC is deeper than that between Nb and Cu in Nb₂CuC, indicating that the Nb–Al bond is more covalent than the Nb–Cu bond. The spherical nature of charge distribution around every element also indicates the presence of some ionic character in chemical bonding of Nb₂CuC and Nb₂AlC.

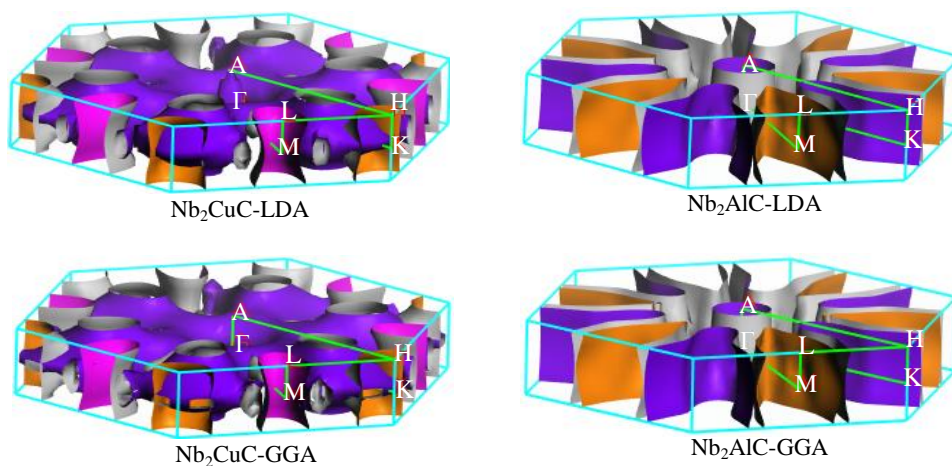


Fig. 7. Fermi surfaces of Nb₂CuC and Nb₂AlC calculated with LDA and GGA functionals.

The FS, an abstract boundary, is helpful for predicting several physical properties such as electrical, thermal, optical and magnetic properties of metals, semi-metals and doped semiconductors. The shape of the FS results from the periodicity and symmetry of the crystalline lattice as well as from the occupied electronic energy bands. The subsistence of a FS is a direct outcome of the Pauli

Exclusion Principle, which permits only one electron per quantum state. The FS can be considered as an energy isosurface in reciprocal space. Since the FS is an unbounded periodic object, it is traditionally illustrated as being cropped by the Brillouin zone. The FS of Nb₂AlC consists of two sheets, whereas that of Nb₂CuC contains three sheets (Fig. 7). The first sheet of Nb₂AlC is complicated. It consists of a central cylindrical part along the Γ -A direction and a wing along every K-H direction. The second sheet is parallel to the M-L direction and appears like the wing of the first sheet. The FSs obtained with GGA and LDA for Nb₂AlC are identical. The first sheet of FS of Nb₂CuC is very complicated; it has nesting nature, which indicates possible superconductivity of Nb₂CuC [56]. This sheet contains six oblate spheroid structures along the K-H direction. The second sheet along the H-K direction intersects six structures of the first sheet. The third sheet along the M-L direction is similar to the second sheet. The FSs due to LDA and GGA functionals are almost identical, although LDA FS contains an additional capsule-like structure along the Γ -A direction. The substitution of Al by Cu modifies the FS of Nb₂AlC. The non-spherical shape of FS indicates the metallic conductivity of both Nb₂CuC and Nb₂AlC [56].

3.3. Mechanical properties

3.3.1. Single-crystal elastic constants

Due to their hexagonal structure, MAX phases Nb₂CuC and Nb₂AlC have six different elastic constants: C_{11} , C_{33} , C_{44} , C_{66} , C_{12} and C_{13} . Five of them are independent, because $C_{66} = (C_{11} - C_{12})/2$. The calculated elastic constants C_{ij} of Nb₂CuC and Nb₂AlC are listed in Table 4.

Table 4. Single-crystal elastic constants C_{ij} and Cauchy pressure $C_{12}-C_{44}$ of Nb₂CuC and Nb₂AlC.

Phase	Method	Single-crystal elastic constants C_{ij} (GPa)					$C_{12}-C_{44}$ (GPa)	Ref.
		C_{11}	C_{33}	C_{44}	C_{12}	C_{13}		
Nb ₂ CuC	LDA	306	265	20	176	162	156	Present study
	GGA	279	252	26	119	113	93	Present study
	GGA	271	295	23	-----	-----	-----	[11]
Nb ₂ AlC	LDA	374	306	154	86	131	-68	Present study
	GGA	332	300	138	75	116	-63	Present study
	GGA	338	293	139	-----	-----	-----	[11]
	GGA	341	310	150	94	117	-56	[54]
	GGA	315	295	139	89	117	-50	[57]
	GGA	310	289	139	90	118	-49	[58]
	GGA	334	324	154	115	149	-39	[59]
	GGA	311	291	135	93	115	-42	[60]

For a hexagonal structure, the following criteria must be met for mechanical stability [61]:

$$C_{11}, C_{33}, C_{44} > 0; C_{11} > |C_{12}|; \text{ and } (C_{11} + C_{12})C_{33} > 2C_{13}C_{13} \quad (1)$$

Both MAX phases considered here fulfill the above conditions and consequently are mechanically stable according to both LDA and GGA calculations. The elastic constants obtained in the present study with the LDA functional are larger than those obtained with GGA for Nb₂AlC. A similar trend is observed for Nb₂CuC, except for C_{44} . This trend is also observed in previous studies on several MAX phases [62,63]. The deviation of C_{ij} for Nb₂AlC within LDA and GGA functionals lies within 2–15%, whereas the range is 6–48% for Nb₂CuC. Dinga *et al.* [11] derived C_{11} , C_{33} and C_{44} for both Nb₂CuC and Nb₂AlC using GGA functionals; both set of results are consistent with the present study. For Nb₂CuC, the large deviations of LDA values of C_{12} (48%) and C_{13} (44%) from their GGA values demand further investigation.

The elastic constants C_{11} and C_{33} measure the ability to resist compression along the a- and c-axes, respectively. The present calculations with both LDA and GGA functionals show that $C_{11} > C_{33}$ for Nb₂CuC and Nb₂AlC, indicating that both compounds are more incompressible along the a-axis. The C_{44} is related to the shear deformation of the material, with a lower C_{44} value indicating a higher ability of the compound to shear. The C_{44} value of Nb₂CuC is about one-seventh of that of Nb₂AlC. Therefore, Nb₂CuC is much more shearable than its precursor Nb₂AlC. High shearability (small C_{44})

of Nb₂CuC is the origin of its higher machinability. Conversely, the large C_{44} of Nb₂AlC indicates that it will strongly resist shear deformation in the (100) plane. The C_{12} and C_{13} are also related to shear stress, and collectively act as an effective stress component along the a-axis together with a uniaxial strain in the b- and c-axes, respectively. The comparatively large values of C_{12} and C_{13} make the Nb₂CuC phase able to resist shear deformation along the b- and c-axes under large stresses along the a-direction.

The difference $C_{12}-C_{44}$ is defined as the Cauchy pressure, which serves as a parameter to describe the mechanical behavior of crystalline solids [64]. Ductile failure is associated with those materials with positive Cauchy pressure and brittle failure with materials exhibiting a negative Cauchy pressure. The Nb₂CuC is ductile, whereas Nb₂AlC is brittle. However, ductile materials (i.e. Nb₂CuC) are inherently damage tolerant. Additionally, positive Cauchy pressure is linked to metallic bonding, but negative Cauchy pressure corresponds to directional covalent bonding. Therefore, Nb₂CuC is dominated by metallic bonding and Nb₂AlC has strong directional covalent bonding. This is consistent with the prediction made by Mulliken population analysis in Section 3.3.2. The directional covalent bonding is the origin of high shearability of Nb₂AlC.

3.3.2. Poly-crystalline elastic moduli

Knowledge of poly-crystalline elastic moduli such as bulk modulus (B), shear modulus (G), Young's modulus (E) and their derivatives Pugh's ratio (B/G) and Poisson's ratio (ν) are important in engineering applications. The B and G are calculated from the well-known Voigt–Reuss–Hill approximations using C_{ij} [65–67]; E and ν are obtained from the following: $E = 9BG/(3B + G)$ and $\nu = (3B - 2G)/(6B + 2G)$. The calculated results are shown in Table 5.

Table 5. Bulk moduli B_V , B_R and B (GPa); shear moduli G_V , G_R and G (GPa); Young's modulus E (GPa), Pugh's ratio (B/G) and Poisson's ratio (ν) of Nb₂CuC and Nb₂AlC.

Phase	Method	B_V	B_R	B	G_V	G_R	G	E	B/G	ν	Ref.
Nb ₂ CuC	LDA	208.44	206.59	207.52	46.40	34.50	40.45	113.95	5.13	0.408	Present study
	GGA	166.83	166.30	166.56	57.61	43.77	50.69	138.06	3.29	0.362	Present study
	GGA			183			44.8	124.26	4.08	0.387	[11]
Nb ₂ AlC	LDA	194.21	193.99	194.10	137.37	132.13	134.75	328.28	1.44	0.218	Present study
	GGA	175.48	175.46	175.47	124.80	121.66	123.23	299.56	1.42	0.215	Present study
	GGA			175			124	301	1.41	0.213	[11]
	GGA			183			131	317	1.40	0.211	[54]
	GGA			174.6			116.3	285.6	1.50	0.227	[57]
	GGA			173			116	285	1.49	0.226	[58]
	GGA	202.0	208.3	205.2	122.2	115.5	118.8	298.8	1.73	0.257	[59]
	GGA	173.22	173.22	173.22	115.13	112.18	113.66	279.79	1.52	0.231	[60]
EXPT			165			117	286	1.41	0.213	[68]	

The elastic moduli obtained in the present study with the LDA functional are larger than those obtained with GGA for Nb₂AlC; elastic moduli obtained with LDA are generally larger than those obtained with GGA [61,62]. In the case of G and E for Nb₂CuC, this tendency of LDA is reversed; this discrepancy indicates the need for further investigation. The deviation of elastic moduli for Nb₂AlC within LDA and GGA functionals lies within 9–11%, while for Nb₂CuC the range is 18–24%. The present GGA values are consistent with previous DFT/GGA studies [11,54,57–60,68].

The bulk moduli of Nb₂CuC and Nb₂AlC are larger than their shear moduli calculated using two different functionals, indicating that the mechanical stability of these compounds is controlled by shear modulus. The LDA value of B for Nb₂CuC is greater than that of Nb₂AlC; however, the GGA value of B for Nb₂CuC is much smaller than that of Nb₂AlC. This trend is also observed for G . The G is correlated with hardness and shear elastic constant C_{44} , and it can also be used to determine the resistance to shear deformation under external forces. The Nb₂CuC is deformed easily and is soft and machinable, due to low G . Conversely, Nb₂AlC is capable of resisting shear deformation and shows superior mechanical strength due to its high G . The E is well correlated with hardness and thermal shock resistance of compounds; E for Nb₂CuC is less than half of the value for Nb₂AlC in both calculations. The larger is E , the greater the hardness of the compound. Therefore, Nb₂CuC is soft and machinable and conversely Nb₂AlC is stiff and mechanically strong. The critical thermal shock resistance (R) has the property $R \propto 1/E$, implying that the lower the E , the better the R . The R is the

prerequisite of a material for use as thermal barrier coating (TBC). The GGA E value of Nb₂CuC (124–138 GPa) is lower than that of a potential TBC material BaZrO₃ (248.6 GPa) [69]. Thus, Nb₂CuC is expected to be a promising TBC material if other parameters such as melting temperature, Debye temperature (θ_b), thermal conductivity, and thermal expansion coefficient and oxidation resistance are appropriate.

The B/G ratio [70] can be used to classify solid materials into two groups: (a) brittle materials with $B/G < 1.75$ and (b) ductile materials with $B/G > 1.75$. Based on this, Nb₂CuC is ductile and Nb₂AlC is brittle in nature.

The ratio ν is another parameter that assesses several physical properties of materials and in particular the stability of solids against shear (low values ν suggest stability against shear) [71]. Thus, Nb₂CuC should be unstable against shear, whereas Nb₂AlC should be stable. The central force acts as an interatomic force in solids whose ν is in the range of 0.25–0.50 and non-central force exists as an interatomic force in solids whose ν lies outside this range [72]. Clearly, the interatomic force in Nb₂CuC is central force; however, it is non-central force in Nb₂AlC, except according to one previous study [59]. Additionally, ν is used to predict the failure mode of solids [73,74]. A material with ν less than a critical value of 0.26 undergoes brittle failure, but a material experiences ductile failure for $\nu > 0.26$. The values of ν indicate that Nb₂CuC is highly ductile and Nb₂AlC is brittle in nature, consistent with B/G . Purely covalent crystals have ν of 0.1 and metallic compounds have ν of 0.33 [75]. Both Nb₂CuC and Nb₂AlC, like other MAX phases, are characterized by a mixture of covalent and metallic nature.

In the new compound Nb₂CuC, the A-group element Al is replaced from Nb₂AlC with the transition metal Cu. The substitution of Al with Cu modifies the band profile of Nb₂CuC. Consequently, Nb₂CuC is highly ductile and damage tolerant, and its G and E decrease considerably; C_{44} representing shear strength also decreases. Damage-tolerant materials have potential applications in aerospace vehicles. Conversely, brittle materials have potential uses as heat sinks, automotive cooling systems, consumer electronic devices, motor and battery housings, heat exchangers and heat sensors.

3.3.3. Elastic anisotropy

Elastic anisotropy refers to the directional dependence of mechanical properties, which are closely related to plastic deformation and cracking behavior of materials. For a comprehensive understanding of elastic anisotropy, we calculate the shear anisotropy factors A_1 , A_2 and A_3 , compressibility anisotropy factor k_c/k_a , percentage anisotropy factors A_B and A_G , and universal anisotropy factor A^U using previously published formulas [76]. Anisotropy factors are listed in Table 6. Elastically isotropic crystals have unit value for A_i ($i = 1-3$) and k_c/k_a . The deviation of these factors from unit value quantifies the level of elastic anisotropy in shear and compression. The factors A_B , A_G and A^U reveal the degree of anisotropy directly, with a zero value indicating the isotropic nature in elasticity. The elastic anisotropy levels calculated for Nb₂CuC and Nb₂AlC are shown in Fig. 8, in which A_B and A_G are expressed in percentage (%) and others in relative unit (ru). All factors show larger elastic anisotropy level for LDA than GGA except for A_2 in Nb₂AlC. In most cases Nb₂CuC is elastically more anisotropic than Nb₂AlC. Only in the shear plane {001}, shear anisotropy in Nb₂AlC is larger than that in Nb₂CuC.

Table 6. Elastic anisotropy factors for Nb₂CuC and Nb₂AlC MAX phases.

Phases	A_1	A_2	A_3	k_c/k_a	A_B	A_G	A^U	Remarks
Nb ₂ CuC	3.033	0.308	0.933	1.534	0.446	14.710	1.734	LDA
	2.885	0.325	0.938	1.237	0.159	13.652	1.584	GGA
Nb ₂ AlC	0.593	1.069	0.634	1.131	0.057	1.944	0.199	LDA
	0.656	1.074	0.704	0.951	0.006	1.274	0.129	GGA

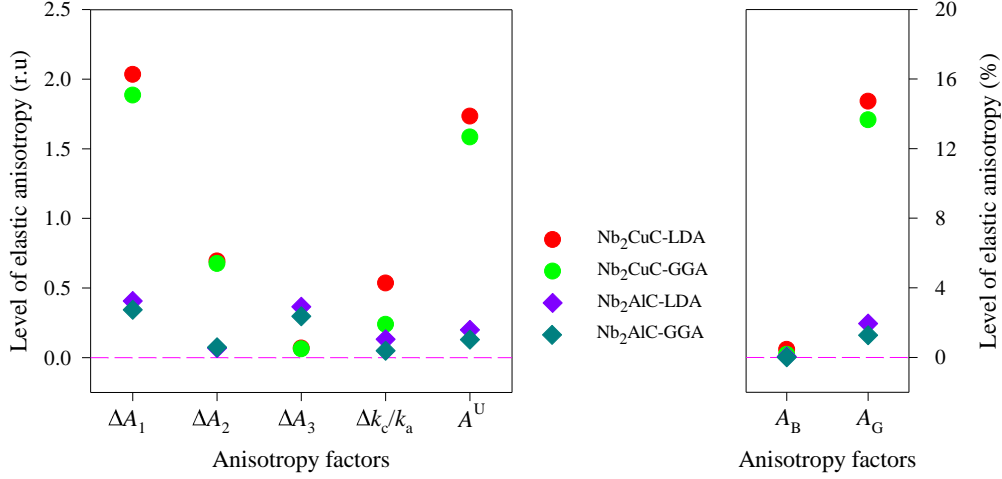


Fig. 8. Level of elastic anisotropy of Nb₂CuC and Nb₂AlC.

3.3.4. Hardness

Hardness is a measure of the resistance to localized plastic deformation of solids induced by either mechanical indentation or scratching. Hardness is related to ductility, elastic stiffness, plasticity, strain, strength and toughness. The correlations between these properties and hardness can provide an understanding of the mechanical behavior of solids. Among three main types of hardness measurements, indentation hardness measurement is used frequently. Indentation hardness measures the resistance of material deformation due to a constant compression load from a sharp object. The Vickers indentation hardness scale is popular, among Rockwell, Shore, Brinell and others. Gao *et al.* [77,78] developed a suitable theoretical model for calculating the Vickers hardness (H_V) of partially metallic binary compounds. This model can also be applied for the more complex MAX phases by using a geometric average of hardness of all binary systems in the MAX phase [79,80]. The theoretical details of hardness calculation are described in recent papers [43,81–84]. Calculated H_V and related parameters are listed in Table 7. The LDA value for H_V is slightly larger than the GGA value for the same system. Section 3.3.1 shows that the total DOS $N(E_F)$ at E_F , obtained with GGA, is slightly larger than that obtained with LDA for both compounds, which is the opposite of the trend for H_V with both functionals. The Nb₂CuC has higher total DOS at E_F and lower H_V compared with Nb₂AlC. Therefore, we conclude that the replacement of Al with Cu from Nb₂AlC causes an increase in total DOS at E_F and a decrease in H_V , resulting in Nb₂CuC being relatively soft, machinable and damage tolerant. The calculated values of H_V lie within the range of 2–8 GPa of measured values for MAX phases [85]. The measured values for Nb₂AlC range within 4.5–6.1 GPa [86,87], which are comparable with the present values.

Table 7. Bond number (n^μ), bond length (d^μ), bond population (P^μ), bond volume (v_b^μ (Å³), bond hardness (H_V^μ), metallic population ($P^{\mu'}$) and Vickers hardness (H_V) of Nb₂CuC and Nb₂AlC.

Compound	Functional	Bond	n^μ	d^μ (Å)	P^μ	$P^{\mu'}$	v_b^μ (Å ³)	H_V^μ (GPa)	H_V (GPa)
Nb ₂ CuC	LDA	Nb–C	4	2.15293	0.98	0.0247	9.0083	18.1259	6.78
		Nb–Cu	4	2.70030	0.44	0.0247	17.7742	2.5387	
	GGA	Nb–C	4	2.17651	1.01	0.0218	9.1542	18.2548	6.28
		Nb–A	4	2.78112	0.42	0.0218	19.0983	2.1594	
Nb ₂ AlC	LDA	Nb–C	4	2.15657	0.97	0.0116	8.6114	19.6030	7.20
		Nb–Al	4	2.83526	0.52	0.0116	19.5686	2.6475	
	GGA	Nb–C	4	2.18220	1.00	0.0109	8.8817	19.2152	7.06
		Nb–A	4	2.88429	0.55	0.0109	20.5083	2.5963	

3.4. Thermal properties

3.4.1. Debye temperature

A simple and rigorous way to calculate the Debye temperature θ_D is the Anderson method [88] among several methods [89–93]. This method uses the resultant sound velocity calculated from the longitudinal and transverse components of the elastic wave velocity [1]. The mass density and sound velocities calculated for the determination of θ_D are listed in Table 8 along with θ_D . The LDA value of θ_D is smaller than the GGA value for Nb₂CuC, but in case of Nb₂AlC, the GGA value of θ_D is greater than the LDA value. The Nb₂CuC is a very exceptional MAX phase as it contains an additional transitional metal at the A-site and so is expected to break the general trend for MAX phases. To reach a final conclusion, more theoretical work with similar pair of compounds, e.g. Ti₂CuC and Ti₂AlC, is required. The θ_D of Nb₂CuC is considerably smaller than that of Nb₂AlC. Low θ_D of Nb₂CuC should lead to low thermal conductivity, as discussed in the following section.

Table 8. Density (ρ in g/cm³), sound velocities (v_l , v_t and v_m in km/s), Debye and melting temperatures (θ_D and T_m in K) and minimum and lattice thermal conductivities (k_{min} and k_{ph} in W/m-K)

Phase	Functional	ρ	v_l	v_t	v_m	θ_D	k_{min}	k_{ph}^*	T_m
Nb ₂ CuC	LDA	8.10	5.6807	2.2344	2.5323	317.5	0.813	1.61	1670
	GGA	7.68	5.5215	2.5690	2.8930	356.3	0.896	3.55	1569
Nb ₂ AlC	LDA	6.66	7.4907	4.4976	4.9751	614.4	1.549	46.41	1935
	GGA	6.35	7.3147	4.4051	4.8714	592.1	1.469	42.97	1800

*Calculated at 300 K.

3.4.2. Minimum thermal conductivity

Minimum thermal conductivity (k_{min}) of a compound is the theoretical lower limit of its intrinsic thermal conductivity at high temperature. The phonons are completely unpaired at high temperature and hence the heat energy is delivered to neighboring atoms. In this case, the mean free path of phonons is equal to the average interatomic distance. Accordingly, different atoms can be substituted in a molecule by an equivalent atom of average atomic mass M/n , where n is the number of atoms in the molecule. In the cell, a single equivalent atom has no optical modes. Clarke deduced the following formula for calculating k_{min} of compounds at high temperature [93]:

$$k_{min} = k_B v_m \left(\frac{n N_A \rho}{M} \right)^{2/3} \quad (2)$$

where, k_B is the Boltzmann constant, v_m is average sound velocity, n is the number of atoms in a molecule, N_A is Avogadro's number, ρ is mass density and M is molecular weight. Calculated values of k_{min} for Nb₂CuC and Nb₂AlC follow the trend of θ_D (Table 8).

3.4.3. Lattice thermal conductivity

The ceramic/metallic properties of MAX phases make the DFT calculation of lattice thermal conductivity (k_{ph}) very complicated. Slack [94] developed a simpler method for calculating k_{ph} , which is suitable for MAX phases as they have partial ceramic character. In this method, k_{ph} is calculated from the empirical formula:

$$k_{ph} = A \frac{M_{av} \theta_D^3 \delta}{\gamma^2 n^{2/3} T} \quad (3)$$

This method is discussed in more detail in a recent paper [1]. The k_{ph} calculated at 300 K is listed in Table 8 and its temperature dependence is shown in Fig. 9. It is evident that k_{ph} decreases with the increase of temperature; at low temperature, the rate of decrease is very significant and at high temperature it is more depressed. The Nb₂AlC is thermally more conductive than Nb₂CuC over the entire temperature range. Interestingly, the k_{ph} of Nb₂CuC is much lower than that of Nb₂AlC even though the k_{ph} of Cu is almost double that of Al. Following the trend of θ_D , the LDA value of k_{ph} is greater than the GGA value in Nb₂AlC, but the GGA value is greater than the LDA value in Nb₂CuC.

The fairly low k_{ph} and θ_{D} of Nb_2CuC are two important factors for its application as a TBC material. To facilitate comparison, the potential TBC material BaZrO_3 , has k_{ph} of 5.75 W/m-K at 298 K, 3.43 W/m-K at 1273 K and 2.81 W/m-K at 1473 K. At these temperatures, the calculated k_{ph} values of Nb_2CuC for LDA (GGA) are 1.62 (3.57), 0.38 (0.84) and 0.33 (0.72) W/m-K, respectively, which are significantly lower than those of BaZrO_3 [69,95]. Considering that for a suitable TBC material, k_{min} should be equal or smaller than the threshold value of 1.25 W/m-K [96], Nb_2CuC should be considered a potential TBC material.

3.4.4. Melting temperature

The melting temperature (T_{m}) of hexagonal crystals like MAX phases can be calculated from the elastic constants via the empirical formula [97]:

$$T_{\text{m}} = 1.5(2C_{11} + C_{33}) + 354 \quad (4)$$

The calculated T_{m} of Nb_2CuC and Nb_2AlC with LDA and GGA are listed in Table 8; the LDA value is larger than the GGA value for both compounds. All values exceed 1500 K, indicating that both MAX phases are good candidate materials for high-temperature applications. The MAX phases are inherently oxidation and creep resistant. Alumina-forming MAX phases have excellent oxidation resistance with upper temperature capability possible upto ~ 1400 °C [98]. The Cu slowly reacts with atmospheric oxygen to form a layer of copper oxide, which, unlike the rust that forms on iron in moist air, protects the underlying metal from further oxidation. Many Cu-alloys have high oxidation resistance due to the presence of alloy additives [99]. The Nb_2CuC is expected to be oxidation resistant, as is Nb_2AlC , which will increase the probability of it becoming a TBC material. Both Nb_2CuC and Nb_2AlC are expected to preserve this oxidation resistance in conjunction with good mechanical and physical properties.

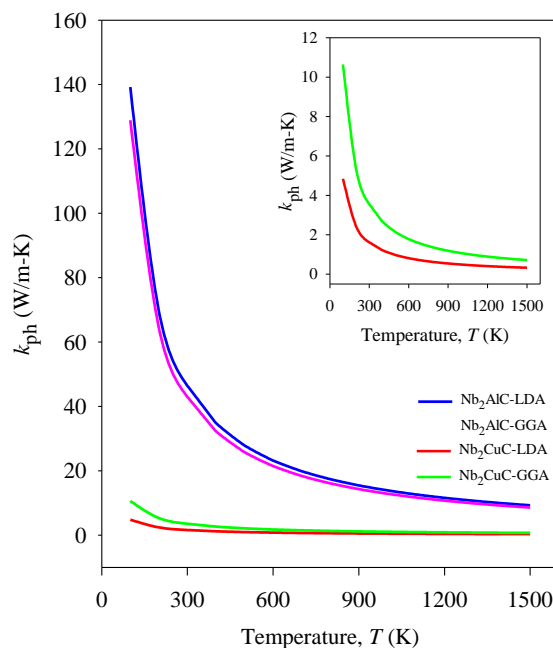


Fig. 9. Lattice thermal conductivity (k_{ph}) as a function of temperature. Inset shows k_{ph} in small scale for Nb_2CuC .

3.5. Dynamical properties

3.5.1. Phonon dispersion

The phonon dispersion spectra investigated for Nb_2CuC and Nb_2AlC are given in Fig. 10. There are no negative frequencies in the phonon spectra of Nb_2CuC and Nb_2AlC in the whole Brillouin zones as seen in Ref. [11], indicating their dynamical stability. Phonon spectra consist of 24 phonon branches

including three acoustic modes and 21 optical modes because the compounds have eight atoms in their unit cells. The lower parts of the phonon spectra indicate the acoustic modes originating from coherent vibration of atoms in a lattice outside their balance positions. The upper parts of the dispersion spectra correspond to the optical modes arising from the out-of-phase oscillations of atoms in a lattice while one atom goes to the left and its neighbor to right. At the Γ -point, the acoustic modes have zero frequency, which also indicates the dynamical stability of Nb_2CuC and Nb_2AlC . These two MAX phases are capable of thermal transport as no band gap arises between acoustic and optical modes due to overlapping. The exchange of A-atom between Nb_2CuC and Nb_2AlC causes a significant change in the dispersion spectra. Acoustic and lower optical branches possess lower frequencies at H, K, M and L symmetry points when Al is substituted by Cu. The phononic band gap between the lower and upper optical branches is reduced when Al is replaced by Cu. The higher optical modes of both compounds possess higher frequencies for the LDA than for the GGA functional.

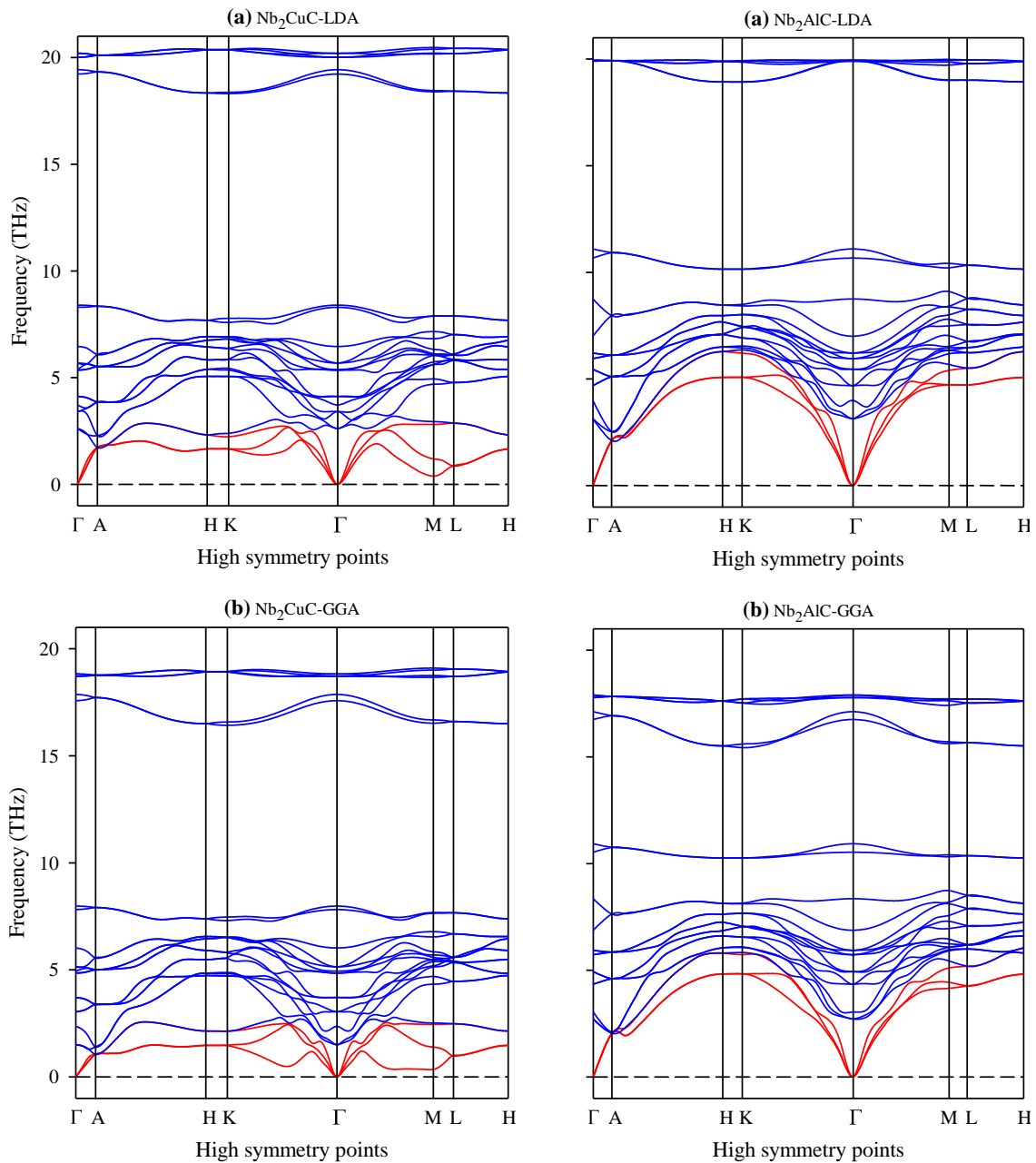


Fig. 10. Phonon dispersion of Nb_2CuC and Nb_2AlC with (a) LDA and (b) GGA functionals. Red and blue indicate the acoustic and optical bands, respectively.

3.5.2. Phonon DOS

Phonon DOS is directly related to the electron–phonon interaction function and also affects the thermodynamic and superconducting properties. Phonon DOS calculated for Nb₂CuC and Nb₂AlC is shown in Fig. 11. The peaks in the phonon DOS at the low-frequency region consist of states from Nb and the A-group atom. These two atoms lead to acoustic and lower optical modes, and C (lighter atom) leads to higher optical modes. Near zero frequency, the main contribution comes from Cu states in Nb₂CuC, but in Nb₂AlC from Nb. The pick on the right side of the lower branch is due to the states of Nb in Nb₂CuC, but in Nb₂AlC this is due to the states of Al. Lower branches shift toward lower frequency regions when Al is substituted by the heavier Cu atom. A narrow band gap in the lower optical branches is observed in the phonon DOS of Nb₂AlC, but no such band gap is found for Nb₂CuC.

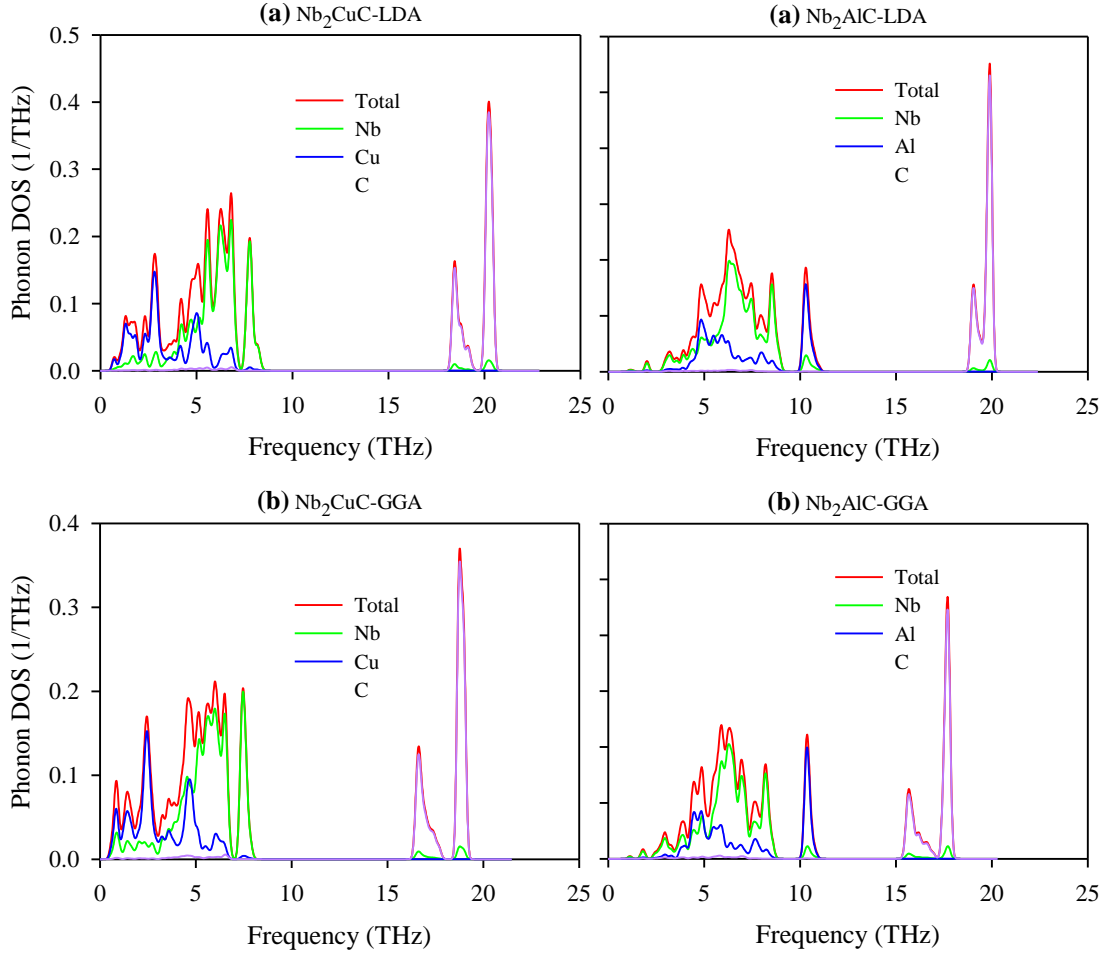


Fig. 11. Phonon DOS of Nb₂CuC and Nb₂AlC with (a) LDA and (b) GGA functionals.

3.5.3. Infrared-and Raman-active modes

Infrared (IR)-active modes are related to non-zero transition dipole moment; in contrast, Raman-active modes are associated with non-zero transition polarizability. Because Nb₂CuC and Nb₂AlC have eight atoms in their unit cells, this leads to 24 vibrational modes at the zone center (Γ -point) including three acoustic and 21 optical modes. In accordance with the factor group, the irreducible representation of the optical modes of Nb₂CuC and Nb₂AlC at Γ -point is as follows [100]:

$$\Gamma_{\text{opt.}} = 2A_{2u} + 4E_{1u} + 4E_{2u} + 2B_{2g} + 4E_{2g} + 2B_{1u} + 2E_{1g} + 1A_{1g}$$

where, E_{1u} and A_{2u} are IR-active modes, and A_{1g} , E_{1g} and A_{2g} are Raman-active modes. The rest of the optical modes (B_{1u} , B_{2g} and E_{2u}) are silent. The MAX phases studied here have seven Raman-active modes ($1A_{1g} + 2E_{1g} + 4E_{2g}$) in sum, consistent with the other 211 MAX phases [1,101].

Table 9 lists the wavenumbers equivalent to frequency as well as energy of IR- and Raman-active modes for each irreducible representation involved in the studied compounds. The molecular polarization potential is modified due to vibrational displacements in a Raman-active mode. The Raman intensity depends on the change of the polarizability prompted by the mode. The Raman-active modes are the Γ -point normal modes, which are controlled by symmetry and selection rules. The identified Raman-active modes A_{1g} , E_{1g} and A_{2g} are the result of simultaneous stretching and then simultaneous compression of bonds, which distort the electron clouds and induce non-zero polarizability. Equally, the identified IR-active modes E_{1u} and A_{2u} are governed by different selection rules. They are involved in change of dipole moment, and consequently optical absorption occurs due to oscillations produced in these modes. For comparison, the Raman-active phonon energies (in cm^{-1}) of Nb_2AlC calculated with GGA function in different code are available in literature [102]. For modes ω_1 , ω_2 , ω_3 and ω_4 , these values are 144, 211, 193 and 251 cm^{-1} , respectively; the corresponding measured values in the literature are 149, 211, 190 and 262.8 cm^{-1} [103]. Both sets of results are consistent with the values listed in Table 9, indicating the reliability of this study.

Table 9. The zone-center optical phonon modes (IR- and Raman-active) with wavenumbers (ω) for Nb_2CuC and Nb_2AlC MAX phases.

Mode	Irr. Rep	ω (cm^{-1})				
		LDA		GGA		
		Nb_2CuC	Nb_2AlC	Nb_2CuC	Nb_2AlC	
IR	ω_1	E_{1u}	137.35	182.11	136.70	164.56
	ω_2	A_{2u}	215.47	355.87	205.27	351.26
	ω_3	E_{1u}	667.50	663.80	585.68	596.99
	ω_4	A_{2u}	648.10	664.22	593.21	571.01
Raman	ω_1	E_{2g}	113.90	156.29	123.61	145.00
	ω_2	E_{2g}	189.62	207.34	190.59	197.93
	ω_3	E_{1g}	178.49	198.56	181.98	191.14
	ω_4	A_{1g}	280.24	291.91	264.61	278.71

3.6. Optical properties

The Nb_2CuC and Nb_2AlC are elastically anisotropic, as discussed in Section 3.3.3. Optically, MAX phases are also anisotropic [38,40,46,104]. Considering this, we investigated optical properties of Nb_2CuC and Nb_2AlC for two different polarization directions $\langle 100 \rangle$ and $\langle 001 \rangle$, which are applicable for hexagonal systems. The results are analyzed in the next sub-sections.

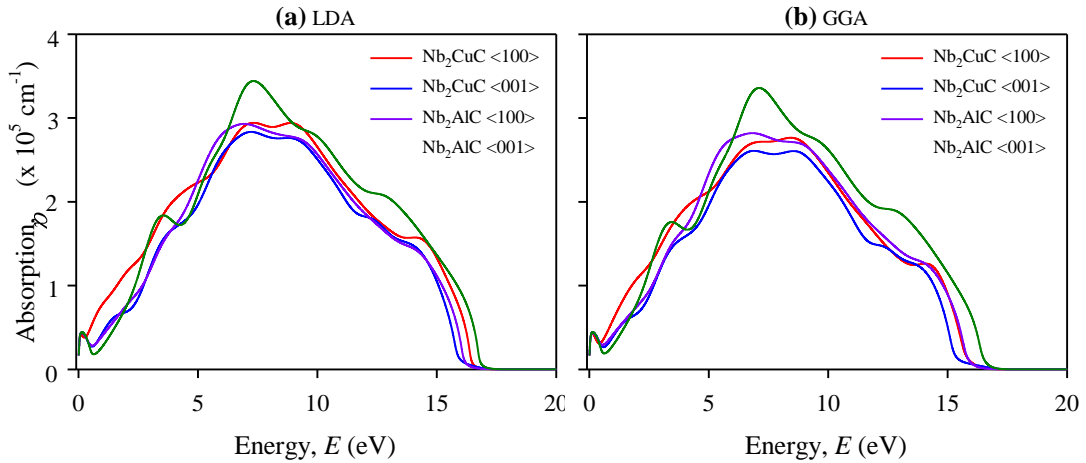


Fig. 12. Optical absorption of Nb_2CuC and Nb_2AlC with (a) LDA and (b) GGA functionals.

3.6.1. Absorption

The optical absorption $\alpha(\omega)$ is a measure of penetration of light at a specific wavelength into a solid before being absorbed. It affords information regarding optimum solar energy conversion efficiency, which is crucial for the practical usage of a material in a solar cell. The optical absorptions investigated along the $\langle 100 \rangle$ and $\langle 001 \rangle$ polarization directions with LDA and GGA functionals are shown in Fig.12. The MAX phases considered here absorb maximum energies of incident light in the photon energy range of 6.8–7.4 eV for both functionals. The light absorption in Nb₂CuC with both functionals is slightly larger for $\langle 100 \rangle$ polarization direction, whereas Nb₂AlC absorbs more light for $\langle 001 \rangle$ polarization, indicating their slight optically anisotropic nature. For photon energy above 16 eV, both compounds absorb no light of any polarization. The spectral features for both functionals are practically similar. It is worth mentioning that the static absorption coefficient $\alpha(0)$ shows a universal non-zero value for studied MAX phases as for other hexagonal systems [105].

3.6.2. Optical conductivity

The optical conductivity is an essential parameter for explaining the electromagnetic response of a material. It implies the electrical conductivity when an alternating electric field exists and links the current density to the electric field for common frequencies. The optical conductivity is a good presumption of the photoconductivity [106]. The real part of optical conductivity calculated for Nb₂CuC and Nb₂AlC for $\langle 100 \rangle$ and $\langle 001 \rangle$ polarization directions with both LDA and GGA is shown in Fig. 13. The spectra for both polarizations show slight change in photon energy range of 0–8 eV for both materials, indicating small anisotropic nature of the optical properties. The shapes of spectra are almost identical except of Nb₂CuC for $\langle 100 \rangle$ polarization with LDA functional. Peak heights are slightly larger for LDA compared with GGA. The peaks in the spectra for both polarization directions arise mainly from the interband transition from the occupied Nb p orbitals to unoccupied Nb d orbitals.

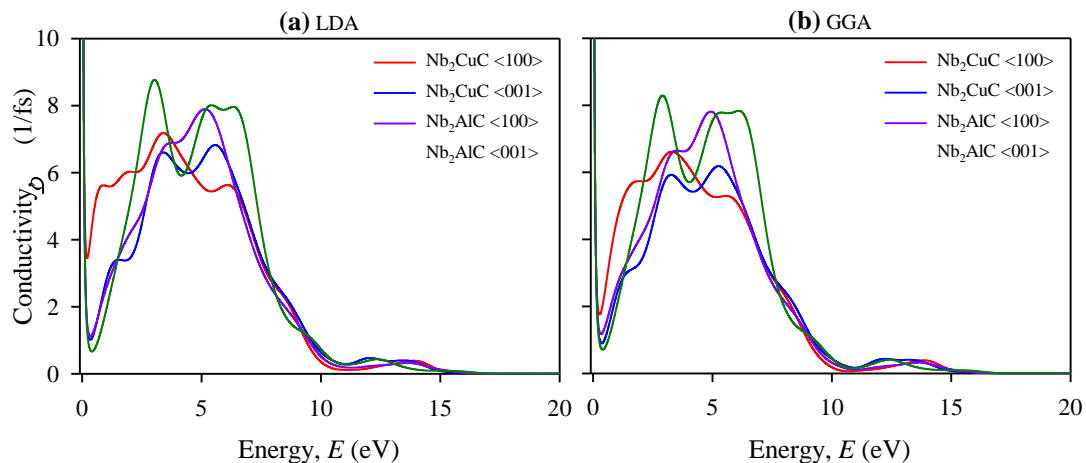


Fig. 13. Optical conductivity of Nb₂CuC and Nb₂AlC with (a) LDA and (b) GGA functionals.

3.6.3 Real part of dielectric constant

The real part of the dielectric constant corresponds to the permittivity component that measures the stored energy and has a directly proportional relationship to the field amplitude, thus it is important for optoelectronic devices. The real part of the dielectric constant calculated for $\langle 100 \rangle$ and $\langle 001 \rangle$ polarization directions for two MAX compounds is shown in Fig. 14. The real part $\epsilon_1(\omega)$ of the dielectric constant passes through zero from below (negative values) in the low-energy region, indicating the metallic nature of the compounds studied here. The Nb₂AlC has the highest dielectric constant at a low energy of ~1.2 eV for $\langle 001 \rangle$ polarization direction with both functionals, whereas Nb₂CuC has almost three times larger dielectric constant at a low energy of ~0.6 eV for $\langle 100 \rangle$ polarization direction for GGA functional than for LDA. For different polarization directions, the

spectra of $\epsilon_1(\omega)$ show different features in the photon energy range of 0–10 eV for both functionals, indicating the optically anisotropic nature of MAX phases.

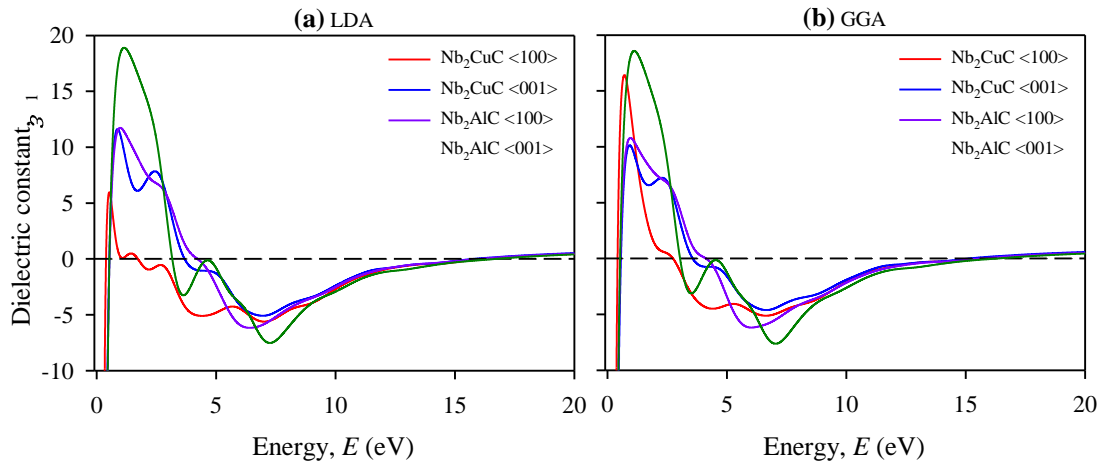


Fig. 14. Real part of the dielectric constant of Nb₂CuC and Nb₂AlC with (a) LDA and (b) GGA functionals.

3.6.4 Imaginary part of dielectric constant

Relating to the optical phenomena, the imaginary part $\epsilon_2(\omega)$ of the dielectric constant reveals the energy attenuation characteristics of the optical system with frequency. The $\epsilon_2(\omega)$ is calculated for Nb₂CuC and Nb₂AlC with both functionals for two polarization directions (Fig. 15). The spectra of $\epsilon_2(\omega)$ for both polarization directions and for both functionals approaches zero from above, indicating the metallic conductivity of the MAX phases studied here. The spectral features for different polarizations differ, but there is no significant difference for the two functionals. Since the band structures are greatly responsible for optical spectra, the origin of peaks in the spectra can be interpreted from the DOS plots of the related compounds. To clarify this correlation, Nb₂CuC was chosen arbitrarily. In the $\langle 001 \rangle$ spectrum with LDA (GGA), the peak around 0.98 eV (1.02 eV) is caused by transitions within Nb 4d bands, and the peak around 3.07 eV (2.93 eV) is due to transitions within C 2p bands.

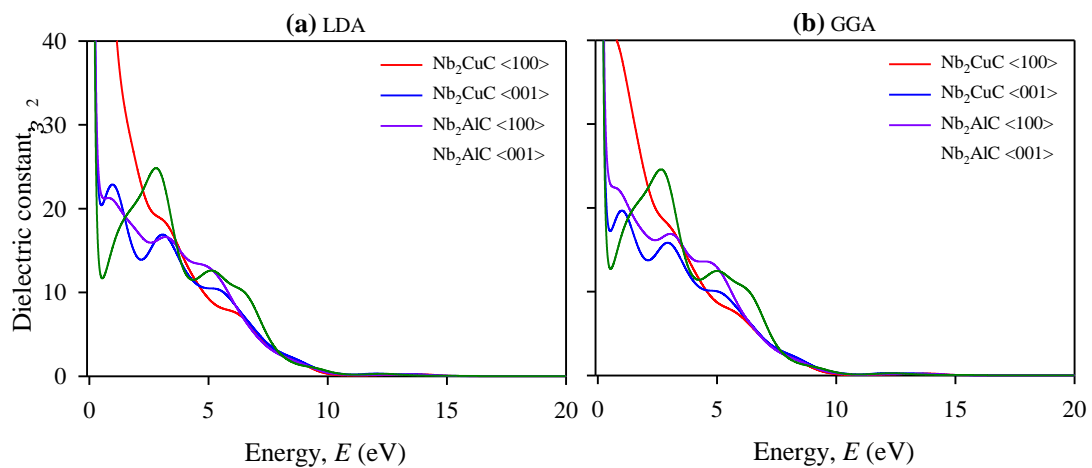


Fig. 15. Imaginary part of the dielectric constant of Nb₂CuC and Nb₂AlC with (a) LDA and (b) GGA functionals.

3.6.5 Loss function

The energy loss function $L(\omega)$ defines the energy loss of the first electron traversing through a material. The $L(\omega)$ values calculated for two MAX phases Nb₂CuC and Nb₂AlC with the GGA and LDA functionals for the $\langle 100 \rangle$ and $\langle 001 \rangle$ polarization directions are shown in Fig. 16. The energy loss spectrum refers to the frequency of collective oscillations of the valence electrons, and its peak

describes the character of plasma oscillation and corresponds to a characteristic frequency known as the plasma frequency (ω_p) of the material. At ω_p , the real part of the dielectric function, $\epsilon_1(\omega)$, changes from negative to positive together with the imaginary part of the dielectric function, $\epsilon_2(\omega) < 1$. At the plasma frequency, the material changes from metallic to dielectric response. From the energy loss spectra, the plasma frequencies of Nb₂CuC and Nb₂AlC with LDA (GGA) are 16.4(15.6) and 16.0 (15.7) eV, respectively, for $\langle 100 \rangle$ polarization; and correspondingly 15.8(15.2) and 16.7(16.4) eV for $\langle 001 \rangle$ polarization. The plasma frequency is slightly smaller for the GGA functional than for the LDA. The plasma frequency of Nb₂CuC for the $\langle 100 \rangle$ polarization is larger than that for the $\langle 001 \rangle$ polarization; conversely, the plasma frequency of Nb₂AlC is larger for the $\langle 001 \rangle$ polarization. The energy loss spectra show no peaks in the energy range of 0–10 eV due to the large $\epsilon_2(\omega)$ [46].

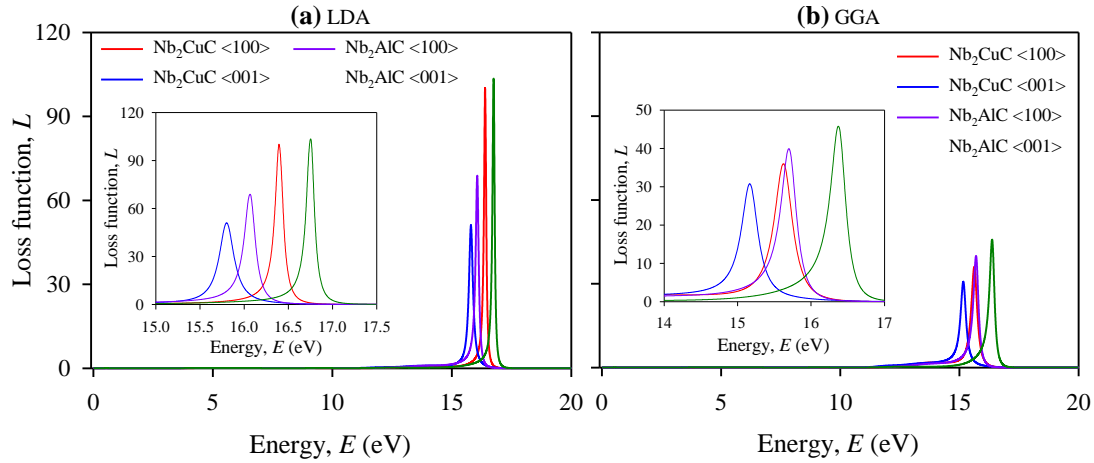


Fig. 16. Loss functions of Nb₂CuC and Nb₂AlC with (a) LDA and (b) GGA functionals.

3.6.6 Reflectivity

The reflectivity of two MAX phases is calculated with two functionals LDA and GGA for $\langle 100 \rangle$ and $\langle 001 \rangle$ polarization directions (Fig. 17). The spectra for both polarizations with LDA and GGA functionals have almost the same shape, but the heights and positions of the peaks differ considerably. In the visible region, the average reflectivity of two compounds for both polarizations with two functionals exceeds 40%, making them candidate materials for coating to reduce solar heating [107]. In the $\langle 100 \rangle$ polarization direction, Nb₂CuC has almost constant reflectivity above 50%, and in this polarization Nb₂CuC is a better coating material for preventing solar heating than Nb₂AlC. In the UV region, both compounds exhibit maximum reflectivity with LDA and GGA functionals at around 11.0 and 10.5 eV for both polarizations, respectively. Above 15 eV, the reflectivity is drastically reduced for both polarizations and functionals.

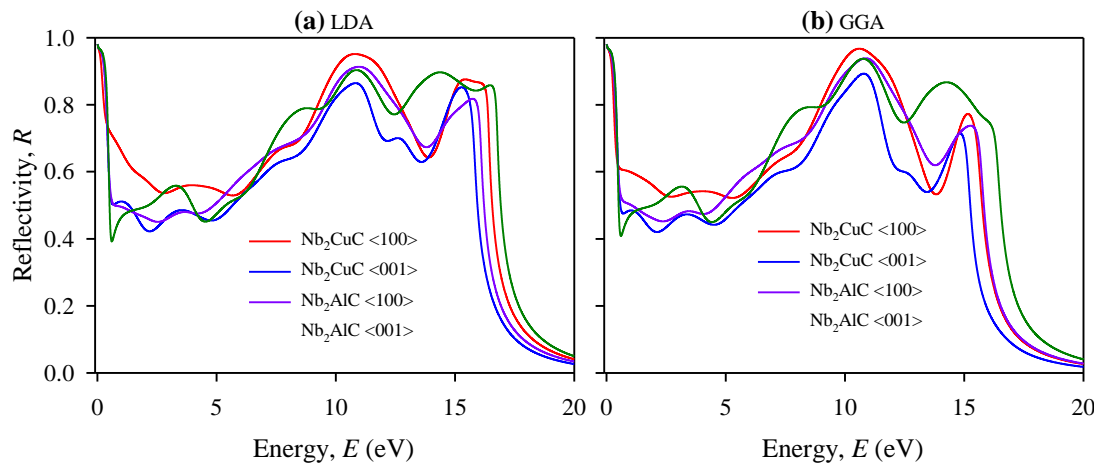


Fig. 17. Reflectivity of Nb₂CuC and Nb₂AlC with (a) LDA and (b) GGA functionals.

3.6.7. Refractive index

Accurate information of the refractive index $n(\omega)$ of materials is an important guide for perfect design of optoelectronic devices. The refractive index of Nb₂CuC and Nb₂AlC MAX phases is calculated with LDA and GGA functionals for $\langle 100 \rangle$ and $\langle 001 \rangle$ polarizations (Fig. 18). For the two MAX phases studied here, the static value of the refractive index $n(0)$ for both polarization directions with both functionals is almost the same, with an approximate value of 84.5. A sharp peak in each spectrum caused by intraband transitions of electrons is observed in the moderate IR region. The $n(\omega)$ spectra show a rapid decrease starting within 0.4–0.7 eV and attain minima at around 10.2 eV. The spectra then remain unchanged up to 16 eV for LDA, and up to 15 eV for GGA, and again increase to reach a value of approximately 0.7 at 20 eV. Although the shapes of the refractive spectra are almost the same, there is evidence of slight anisotropy in the whole energy range.

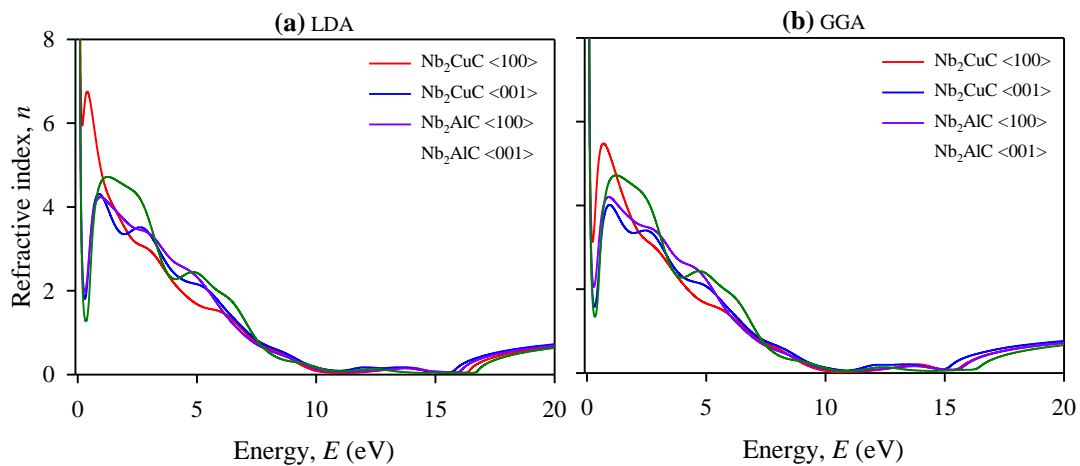


Fig. 18. Refractive index of Nb₂CuC and Nb₂AlC with (a) LDA and (b) GGA functionals.

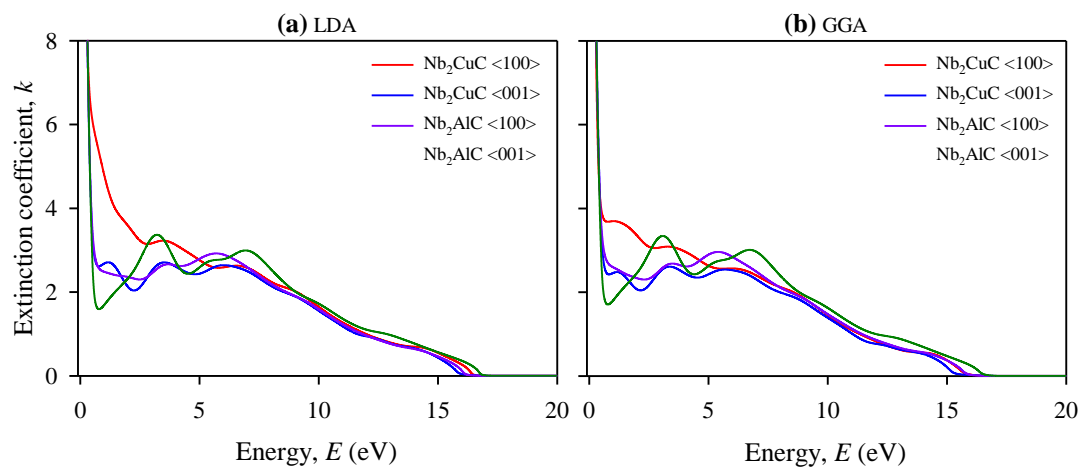


Fig. 19. Extinction coefficient of Nb₂CuC and Nb₂AlC with (a) LDA and (b) GGA functionals.

3.6.8. Extinction coefficient

The extinction coefficient $k(\omega)$, the imaginary part of the complex index of refraction, can serve as an essential key optical parameter. It is related to the attenuation of electromagnetic radiation in a medium and describes how intensely a material absorbs light at a specific wavelength per mass density or per molar concentration. The $k(\omega)$ of Nb₂CuC and Nb₂AlC MAX phases calculated with LDA and GGA functionals for the $\langle 100 \rangle$ and $\langle 001 \rangle$ polarizations are given in Fig. 19. The $k(\omega)$ is related to the conductive properties of materials. A metallic material has a large $k(\omega)$, but a semiconductor has a small $k(\omega)$. Conversely, a dielectric material is essentially a non-conductor with

$k(\omega) = 0$. A large $k(\omega)$ at low photon energy indicates metallic conductivity of the two MAX phases studied here. The spectra of $k(\omega)$ for both functionals are almost the same. Only $k(\omega)$ of Nb₂CuC for $\langle 100 \rangle$ shows different features at low photon energies. The spectra for different polarizations show slight anisotropic features.

4. Conclusions

This is a systematic DFT study of the properties of the recently discovered 211 MAX phase Nb₂CuC, in particular the structural, electronic, elastic, thermal, vibrational and optical properties using two functionals (LDA and GGA). To facilitate comparison, calculations for the isostructural 211 MAX phase Nb₂AlC are also performed. For most properties considered, the GGA functional exhibits better agreement with experimental results. The introduction of Cu in the A-site leads to improved physical properties; Nb₂CuC is ductile and consequently damage tolerant, but Nb₂AlC is brittle. The Nb₂CuC is relatively soft, machinable and more elastically anisotropic. Both are mechanically and dynamically stable and oxidation resistant. The Nb₂CuC is more metallic than Nb₂AlC; Nb₂CuC has a lower θ_D ; and Nb₂AlC is thermally more conductive than Nb₂CuC. Importantly, Nb₂CuC is expected to be a promising TBC material. Nesting nature in the FS is an indication of possible superconductivity of Nb₂CuC.

Data availability: Supplementary data will be made available on request.

Declaration: There is no conflict of interest to declare.

Credit authorship contribution statement

M.A. Hadi: Data curation, investigation, methodology, formal analysis and writing original draft. **N. Kelaidis:** Investigation and formal analysis. **S.H. Naqib:** Formal analysis, conceptualization and project administration. **A.K.M.A. Islam:** Formal analysis, review and editing. **A. Chroneos:** Formal analysis, writing, review and editing. **R.V. Vovk:** Formal analysis.

References

- [1] M.A. Hadi, J. Phys. Chem. Solids 138 (2020) 109275.
- [2] M.W. Barsoum, Prog. Solid. State Chem. 28 (2000) 201–281.
- [3] M. Sokol, V. Natu, S. Kota, M.W. Barsoum, Trends in Chemistry 1 (2019) 210–223.
- [4] T. Rackl, L. Eisenburger, R. Niklaus, D. Johrendt, Phys. Rev. Mater. 3 (2019) 054001.
- [5] M. Radovic, M.W. Barsoum, Am. Ceram. Soc. Bull. 92 (2013) 20–27.
- [6] M.A. Hadi, N. Kelaidis, S.H. Naqib, A. Chroneos, A.K.M.A. Islam, Comp. Mater. Sci. 168 (2019) 203–212.
- [7] D.J. Tallman, E.N. Hoffman, E.N. Caspi, B.L. Garcia-Diaz, G. Kohse, R.L. Sindelar, M.W. Barsoum, Acta Materialia 85 (2015) 132–143.
- [8] Y. Bai, N. Srikanth, C.K. Chua, K. Zhou, Critical Review in Solid State and Materials Science 44 (2019) 56–107.
- [9] M.A. Hadi, M.A. Rayhan, S.H. Naqib, A. Chroneos, A.K.M.A. Islam, Comp. Mater. Sci. 170 (2019) 109144.
- [10] M. Li, J. Lu, K. Luo, Y. Li, K. Chang, K. Chen, J. Zhou, J. Rosen, L. Hultman, P. Eklund, P.O.Å. Persson, S. Du, Z. Chai, Z. Huang, Q. Huang, J. Am. Chem. Soc. 141 (2019) 4730–4737.
- [11] H. Dinga, Y. Li, J. Lu, K. Luo, K. Chen, M. Li, P.O.A. Persson, L. Hultman, P. Eklund, S. Du, Z. Huang, Z. Chai, H. Wang, P. Huang, Q. Huang, Mater. Res. Lett. 7 (2019) 510–516.

- [12] S.J. Clark, M.D. Segall, C.J. Pickard, P.J. Hasnip, M.I.J. Probert, K. Refson, M.C. Payne, Z. Kristallogr. 220 (2005) 567.
- [13] P. Hohenberg, W. Kohn, Phys. Rev. 136 (1964) B864.
- [14] W. Kohn, L.J. Sham, Phys. Rev. 140 (1965) A1133.
- [15] D.M. Ceperley, B.J. Alder, Phys. Rev. Lett. 45 (1980) 566.
- [16] J.P. Perdew, A. Zunger, Phys. Rev. B 23 (1981) 5048.
- [17] J.P. Perdew, J.A. Chevary, S.H. Vosko, K.A. Jackson, M.R. Pederson, D.J. Singh, C. Fiolhais, Phys. Rev. B 48 (1993) 4978.
- [18] J.P. Perdew, K. Burke, M. Ernzerhof, Phys. Rev. Lett. 77 (1996) 3865–3868.
- [19] D. Vanderbilt, Phys. Rev. B 41 (1990) 7892.
- [20] T.H. Fischer, J. Almlof, J. Phys. Chem. 96 (1992) 9768.
- [21] H.J. Monkhorst, J.D. Pack, Phys. Rev. B 13 (1976) 5188.
- [22] F.D. Murnaghan, Finite Deformation of an Elastic Solid (Wiley, New York, 1951).
- [23] M.A. Hadi, M. Roknuzzaman, A. Chroneos, S.H. Naqib, A.K.M.A. Islam, R.V. Vovk, K. Ostrikov, Comp. Mater. Sci. 137 (2017) 318–326.
- [24] S.-R.G. Christopoulos, P.P. Filippatos, M.A. Hadi, N. Kelaidis, M.E. Fitzpatrick, A. Chroneos, J. Appl. Phys. 123 (2018) 025103.
- [25] P.P. Filippatos, M.A. Hadi, S.-R.G. Christopoulos, A. Kordatos, N. Kelaidis, M.E. Fitzpatrick, M. Vasilopoulou, A. Chroneos, Materials 12 (2019) 4098.
- [26] M.A. Hadi, M.A. Alam, M. Roknuzzaman, M.T. Nasir, A.K.M.A. Islam, S.H. Naqib, Chin. Phys. B 24 (2015) 117401
- [27] M.A. Hadi, M.T. Nasir, M. Roknuzzaman, M.A. Rayhan, S.H. Naqib, A.K.M.A. Islam, Phys. Status Solidi B 253 (2016) 2020–2026.
- [28] M.A. Hadi, M.S. Ali, S.H. Naqib, A.K.M.A. Islam, Chin. Phys. B 26 (2017) 037103.
- [29] M.A. Alam, M.A.K. Zilani, F. Parvin, M.A. Hadi, Int. J. Mod. Phys. B 31 (2017) 1750135.
- [30] M.A. Ali, M.A. Hadi, M.M. Hossain, S.H. Naqib, A.K.M.A. Islam, Phys. Status Solidi B 254 (2017) 1700010.
- [31] Mirza H.K. Rubel, M.A. Hadi, M.M. Rahaman, M.S. Ali, M. Aftabuzzaman, R. Parvin, A.K.M.A. Islam, N. Kumada, Comp. Mater. Sci. 138 (2017) 160–165.
- [32] M.T. Nasir, M.A. Hadi, M.A. Rayhan, M.A. Ali, M.M. Hossain, M. Roknuzzaman, S.H. Naqib, A.K.M.A. Islam, M.M. Uddin, K. Ostrikov, Phys. Status Solidi B 254 (2017) 1700336.
- [33] A.M.M. Tanveer Karim, M.A. Hadi, M.A. Alam, F. Parvin, S.H. Naqib, A.K.M.A. Islam, J. Phys. Chem. Solids 117 (2018) 139–147.
- [34] M.A. Hadi, M.N. Islam, M.H. Babu, Z. Naturforsch. A 74 (2019) 71.
- [35] M. N. Islam, M.A. Hadi, J. Podder, AIP Advances 9 (2019) 125321
- [36] R.S. Mulliken, J. Chem. Phys. 23 (1955) 1833.
- [37] D. Sanchez-Portal, E. Artacho, J.M. Soler, Solid State Commun. 95 (1995) 685.
- [38] M.A. Hadi, R.V. Vovk, A. Chroneos, J. Mater. Sci. Mater. Electron. 27 (2017) 11925–11933.
- [39] I. Salama, T. El-Raghy, M.W. Barsoum, J Alloy Compd. 347 (2002) 271–278.
- [40] M.A. Hadi, M.S. Ali, S.H. Naqib, A.K.M.A. Islam, Int. Journal of Computational Materials Science and Engineering 2 (2013) 1350007.
- [41] M.T. Nasir, M.A. Hadi, S.H. Naqib, F. Parvin, A.K.M.A. Islam, M. Roknuzzaman, M.S. Ali, International Journal of Modern Physics B 28 (2014) 1550022,
- [42] M. Roknuzzaman, M.A. Hadi, M.J. Abedin, M.T. Nasir, A.K.M.A. Islam, M.S. Ali, K. Ostrikov, S.H. Naqib, Computational Materials Science 113 (2016) 148–153.
- [43] M.A. Hadi, Computational Materials Science 117 (2016) 422–427.
- [44] M.A. Hadi, M.S. Ali, Chinese Physics B 25 (2016) 107103.
- [45] M.A. Hadi, S.H. Naqib, S.-R.G. Christopoulos, A. Chroneos, A.K.M.A. Islam, Journal of Alloys and Compounds 724 (2017) 1167–1175.
- [46] M. Roknuzzaman, M.A. Hadi, M.A. Ali, M.M. Hossain, N. Jahan, M.M. Uddin, J.A. Alarco, K. Ostrikov, Journal of Alloys and Compounds 727 (2017) 616–626.

- [47] M.A. Hadi, S.-R.G. Christopoulos, S.H. Naqib, A. Chroneos, M.E. Fitzpatrick, A.K.M.A. Islam, *Journal of Alloys and Compounds* 748 (2018) 804–813.
- [48] M.A. Hadi, U. Monira, A. Chroneos, S.H. Naqib, A.K.M.A. Islam, N. Kelaidis, R.V. Vovk, *Journal of Physics and Chemistry of Solids* 132 (2019) 38–47.
- [49] D. Music, Z. Sun, J.M. Schneider, *Phys. Rev. B* 71 (2005) 092102.
- [50] C.D. Gelatt, Jr., A.R. Williams, V.L. Moruzzi, *Phys. Rev. B* 27 (1983) 2005.
- [51] Y. Mo, P. Rulis, W.Y. Ching, *Phys. Rev. B* 86 (2012) 165122.
- [52] S.E. Lofland, J.D. Hettinger, K. Harrell, P. Finkel, S. Gupta, M.W. Barsoum, G. Hug, *Appl. Phys. Lett.* 84 (2004) 508–510.
- [53] A.-J. Xu, W.-W. Zhong, X. Zhang, *Computational Condensed Matter* 6 (2016) 1–4.
- [54] J. Wang and Y. Zhou, *Phys. Rev. B* 69 (2004) 214111.
- [55] M.W. Barsoum, T.El-Raghy, W.D. Porter, H. Wang, J.C. Ho, S. Chakraborty, *J. Appl. Phys.* 88 (2000) 6313–6316.
- [56] S.B. Dugdale, *Phys. Scr.* 91 (2016) 053009.
- [57] W.-Y. Ching, Y. Mo, S. Aryal, P. Rulis, *J. Am. Ceram. Soc.* 96 (2013) 2292–2297.
- [58] M.F. Cover, O. Warschkow, M.M.M. Bilek, D.R. McKenzie, *J. Phys. Condens. Matter* 21(2009) 305403.
- [59] Z. Sun, S. Li, R. Ahuja, J.M. Schneider, *Solid State Communications* 129 (2004) 589–592.
- [60] M. de Jong, W. Chen, T. Angsten, A. Jain, R. Notestine, A. Gamst, M. Sluiter, C.K. Ande, S. van der Zwaag, J.J. Plata, C. Toher, S. Curtarolo, G. Ceder, K.A. Persson, M. Asta, *Scientific Data* 2 (2015) 150009.
- [61] M. Born, *On the stability of crystal lattices. I*, *Mathematical Proceedings of the Cambridge Philosophical Society*, Cambridge University Press, 1940, pp. 160.
- [62] A. Bouhemadou, *Solid State Sciences* 11 (2009) 1875–1881.
- [63] H. Li, G. Sun, J. Deng, W. Zhang, L. Xu, W. Jiang, Y. Feng, K. Li, *Solid State Communications* 204 (2015) 37–40.
- [64] D.G. Pettifor, *Mater. Sci. Technol.* 8 (1992) 345.
- [65] W. Voigt, *Lehrbuchder Kristallphysik*, Teubner, Leipzigund Berlin. 1928.
- [66] A. Reuss, *Z. Angew. Math. Mech.* 9 (1929) 49.
- [67] R. Hilk, *Proc. Phvs. Soc. A* 65 (1952) 349.
- [68] J.D. Hettinger, S.E. Lofland, P. Finkel, T. Meehan, J. Palma, K. Harrell, S. Gupta, A. Ganguly, T. El-Raghy, M.W. Barsoum, *Phys. Rev. B*, 72 (2005)115120.
- [69] Y. Liu, W. Zhang, B. Wang, L. Sun, F. Li, Z. Xue, G. Zhou, B. Liu, H. Nian, *Ceramics International* 44 (2018) 16475–16482.
- [70] S.F. Pugh, *Philos. Mag.* 45 (1954) 823–843.
- [71] P. Ravindran, L. Fast, P.A. Korzhavyi, B. Johansson, J. Wills, O. Eriksson, *J. Appl. Phys.* 84 (1998) 4892.
- [72] O.L. Anderson, H.H. Demarest Jr., *J. Geophys. Res.* 76 1349 (1971).
- [73] I.N. Frantsevich, F.F. Voronov, S.A. Bokuta, *Elastic Constants and Elastic Moduli of Metals and Insulators Handbook* (Naukova Dumka, Kiev, 1983), pp. 60–180.
- [74] G. Vaitheeswaran, V. Kanchana, A. Svane, A. Delin, *J. Phys. Condens. Matter* 19 326214 (2007).
- [75] A. Savin, D.C.H. Flad, J. Flad, H. Preuss, H.G. Schnering, *Angew. Chem. Int. Ed.* 31 (1992) 185–187.
- [76] M.A. Hadi, N. Kelaidis S.H. Naqib, A. Chroneos, A.K.M.A. Islam, *J. Phys. Chem. Solids* 129 (2019) 162–171.
- [77] F. Gao, *Phys. Rev. B* 73 (2006) 132104.
- [78] H. Gou, L. Hou, J. Zhang, F. Gao, *Appl. Phys. Lett.* 92 (2008) 241901.
- [79] A. Szymanski, J.M. Szymanski, *Hardness Estimation of Minerals Rocks and Ceramic Materials* (Elsevier, Amsterdam, 1989).
- [80] V.M. Glazov, V.N. Vigdorovid, *Hardness of Metals* (Izd. Metallurgiya, Moskva, 1989).

- [81] E. Zapata-Solvas, M.A. Hadi, D. Horlait, D.C. Parfitt, A. Thibaud, A. Chroneos, W.E. Lee, J. Am. Ceram. Soc. 100 (2017) 3393.
- [82] M. Mozahar Ali, M.A. Hadi, M.L. Rahman, F.H. Haque, A.F.M.Y. Haider, M. Aftabuzzaman, J. Alloys and Compounds 821 (2020) 153547.
- [83] M.A. Hadi, M. Roknuzzaman, F. Parvin, S.H. Naqib, A.K.M.A. Islam, M. Aftabuzzaman, J. Sci. Res. 6 (2014) 11-27.
- [84] M.A. Alam, M.A. Hadi, M.T. Nasir, M. Roknuzzaman, F. Parvin, M.A.K. Zilani, A.K.M.A. Islam, S.H. Naqib, J. Supercond. Nov. Magn. 29 (2016) 2503–2508.
- [85] M.W. Barsoum, M. Radovic, Annu. Rev. Mater. Res. 41 (2011) 195–227.
- [86] I. Salama, T. El-Raghy, M.W. Barsoum, J. Alloy. Comp. 347 (2002) 271.
- [87] W. Zhang, N. Travitzky, C. Hu, Y. Zhou, P. Greil, J. Am. Ceram. Soc. 92 (2009) 2396–2399.
- [88] O.L. Anderson, J. Phys. Chem. Solids 24 (1963) 909.
- [89] A. Konti, Y.P. Varshni, Canadian Journal of Physics 47 (1969) 2021.
- [90] M.M. Shukla, N.T. Padial, Revista Brasileira de Física 3 (1973) 39.
- [91] Q. Chen, B. Sundman, Acta mater. 49 (2001) 947–961.
- [92] C.V. Somasundari, N.N. Pillai, IOSR Journal of Applied Physics 3, (2013) 01–07.
- [93] D.R. Clarke, Surf. Coat. Technol. 163 (2003) 67–74.
- [94] D.T. Morelli, G.A. Slack, in High Thermal Conductivity Materials, edited by S.L. Shinde and J.S. Goela, Springer, New York, 2006, pp. 37–68.
- [95] R. Vaßen, M.O. Jarligo, T. Steinke, D.E. Mack, D. Stöver, Surf. Coat. Technol. 205 (2010) 938–942.
- [96] Y. Liu, V.R. Cooper, B. Wang, H. Xiang, Q. Li, Y. Gao, J. Yang, Y. Zhou, B. Liu, Mater. Res. Lett. 7 (2019) 145–151.
- [97] M.E. Fine, L.D. Brown, H.L. Mercus, Scr. Metall. 18 (1984) 951–956.
- [98] J.L. Smialek: Unusual Oxidative Limitations for Al-MAX Phases. NASA/TM—2017-219444, Cleveland, OH, 2017.
- [99] M. Walkowicz, P. Osuch, B. Smyrak, T. Knych, E. Rudnik, Ł. Cieniek, A. Róžańska, A. Chmielarczyk, D. Romaniszyn, M. Bulanda, Corrosion Science 140 (2018) 321–332.
- [100] O. Chaix-Pluchery, A. Thore, S. Kota, J. Halim, C. Hu, J. Rosen, T. Ouisse M.W. Barsoum, J. Raman Spectrosc. 48 (2017) 631–638.
- [101] A. Champagne, F. Bourdarot, P. Bourges, P. Piekarczyk, D. Pinek, I. Gélard, J.-C. Charlier, T. Ouisse, Mater. Res. Lett. 6 (2018) 378–383.
- [102] O.D. Leaffer, S. Gupta, M.W. Barsoum, J.E. Spanier, J. Mater. Res. 22 (2007) 2651.
- [103] J.E. Spanier, S. Gupta, M. Amer, M.W. Barsoum, Phys. Rev. B 71, (2005) 012103.
- [104] M.A. Hadi, Y. Panayiotatos, A. Chroneos, J. Mater. Sci. Mater Electron 28 (2017) 3386–3393.
- [105] N. Dhar, D. Jana, J. Phys. Chem. Solids 115 (2018) 332–341.
- [106] G. Yu, H. Lee, A. J. Heeger, S.-W. Cheong, Physica C: Superconductivity 203 (1992) 419-425.
- [107] S. Li, R. Ahuja, M.W. Barsoum, P. Jena, B. Johansson, Appl. Phys. Lett. 92 (2008) 221907.